

# UC San Diego

## UC San Diego Electronic Theses and Dissertations

### Title

Investigation of SUMOylation as a Target to Induce Cures for Head and Neck Cancer

### Permalink

<https://escholarship.org/uc/item/82c6761t>

### Author

Kuang, Yixuan

### Publication Date

2024

Peer reviewed|Thesis/dissertation

UNIVERSITY OF CALIFORNIA SAN DIEGO

Investigation of SUMOylation as a Target to Induce Cures for Head and Neck Cancer

A Thesis submitted in partial satisfaction of the requirements  
for the degree Master of Science

in

Chemistry

by

Yixuan Kuang

Committee in charge:

Professor Yuan Chen, Chair  
Professor Elizabeth Komives, Co-Chair  
Professor Wei Wang

2024

Copyright

Yixuan Kuang, 2024

All rights reserved.

The Thesis of Yixuan Kuang is approved, and it is acceptable in quality and form for publication on microfilm and electronically.

University of California San Diego

2024

## TABLE OF CONTENTS

THESIS APPROVAL PAGE .....	iii
TABLE OF CONTENTS .....	iv
LIST OF FIGURES .....	v
ACKNOWLEDGEMENTS .....	vi
ABSTRACT OF THE THESIS .....	vii
Chapter 1 INTRODUCTION .....	1
Chapter 2 METHODS and MATERIALS .....	7
Chapter 3 RESULTS .....	14
Chapter 4 CONCLUSIONS and FUTURE DIRECTIONS .....	40
REFERENCES .....	42

## LIST OF FIGURES

Figure 3-1. Western blot for SUMOylation in human and murine HNSCC cell line. ....	15
Figure 3-2. Evaluation of the effect of SUMOylation inhibition in the 4MOSC1 murine model. ....	17
Figure 3-3. Single cell transcriptomic analysis of the 4MOSC1 tumors.....	21
Figure 3-4. Single cell transcriptomic analysis of T cells. ....	23
Figure 3-5. Flow cytometry analysis of 4MOSC1 tumors. ....	28
Figure 3-6. Regulation of MHC-I expression on tumor cells by SUMOylation inhibition. ....	31
Figure 3-7. Evaluation of the efficacy of the combination of SUMOylation inhibition with anti-PD1 ICI. ....	36

## ACKNOWLEDGEMENTS

I would like to acknowledge Professor Yuan Chen and Professor Elizabeth Komives for their support as the chair/co-chair of my committee. Their guidance has proved invaluable through multiple drafts and many long nights.

I would like to thank Dai-hua (Debbie) Chen in Chen's lab for her collaboration on the analysis of single-cell RNA-Seq data.

ABSTRACT OF THE THESIS

Investigation of SUMOylation as a Target to Induce Cures for Head and Neck Cancer

by

Yixuan Kuang

Master of Science in Chemistry

University of California San Diego, 2024

Professor Yuan Chen, Chair  
Professor Elizabeth Komives, Co-Chair

Many studies to date are centered on how SUMOylation promotes cancer cells proliferation, but emerging information suggests that SUMOylation also regulates anti-tumor immune response and the tumor microenvironment. Here, with a clinical-stage small molecular SUMOylation inhibitor, TAK-981, I investigated the effects of SUMOylation inhibition in immune-competent mouse models of head and neck cancers. TAK-981 treatment of the mouse significantly prolonged survival and induced completed regression in some cases. The “cured” mice are resistant to rechallenge with the same tumor cells, indicating the formation of immunological memory. Single-cell transcriptomic analysis showed that treatment with the SUMOylation inhibitor decreased terminal exhausted T cells and increased T helper cells in the tumor microenvironment. Besides immune cells, I observed that the SUMOylation inhibitor synergized with IFN- $\gamma$  in upregulating major histocompatibility complex (MHC) class I, which is essential for presenting neoantigen on cancer cells. Based on these findings, I performed combination therapy of the SUMOylation inhibitor with an immune checkpoint inhibitor (anti-PD1) that showed improved efficacy than the monotherapy groups.

## Chapter 1 INTRODUCTION

Small Ubiquitin-like Modifier (SUMO), a protein, and the process of adding SUMO to target protein (SUMOylation) were discovered in 1995<sup>1</sup>, and previous studies discovered that it has prominent functions in cellular regulation of transcription, DNA repair, cell cycle progression, protein translocation<sup>2</sup>. In SUMOylation, a SUMO protein is covalently attached to a target protein via the catalysis by multiple enzymes, including the E1 activating enzyme, the E2 conjugating enzyme, and the E3 SUMO ligase. Briefly, a SUMO-specific E1 activating enzyme activates the C terminus of a mature SUMO protein, forming a SUMO-adenylate conjugate<sup>3,4</sup>. Then, the activated SUMO protein is transferred from the E1 activating protein to the E2 conjugating enzyme with the formation of a thioester linkage<sup>3,5,6</sup>. Finally, SUMO E3 ligases transfer a SUMO protein to the target protein by forming an isopeptide bond between the SUMO protein's C-terminus and a Lys side chain on a target protein<sup>3</sup>. SUMOylation is reversible by different SUMO-specific proteases that are also known as sentrin-specific proteases (SENPs)<sup>3,7,8</sup>. With this reversible post-translational modification on the target proteins, the SUMO proteins and SUMOylation process can regulate many aspects in cells. Since SUMOylation is widespread in all types of cells, there have been many studies about how SUMOylation affects cancer cells since 1995. Still, the functions of SUMOylation in immune cells remain poorly understood, especially in anti-tumor immune response<sup>9</sup>.

TAK-981, a SUMOylation small molecular inhibitor, was developed by Takeda Pharmaceuticals. Through covalently binding to a SUMO protein and non-covalently binding to thereby terminating the SUMOylation process<sup>10</sup>. In a previous study on the effect of TAK-981 in anti-tumor immune response, it was found that TAK-981 can activate dendritic cells to promote T cell priming<sup>11</sup>. Also, it was shown that TAK-981 synergizes with an immune checkpoint

inhibitor (anti-PD1) in a colorectal cancer model<sup>11</sup>. However, because immune cell infiltration and neoantigen development are dependent on tumor types and the organs where they are located, studies of anti-tumor immune response need to be carried out in additional tumor types. In studies presented in this thesis, I investigated the role of TAK-981 in the modulation of tumor cells, tumor immune microenvironment, and tumor-draining lymph nodes in head and neck syngeneic models.

Head and neck squamous cell carcinomas (HNSCC) or head and neck cancer, in short, generally represent a type of cancer that occurs in the oral cavity, pharynx, and larynx. Head and neck cancer was the seventh most common cancer around the world<sup>12</sup>. In 2023, new cases of head and neck cancer rose to 54,540 people, including 39,290 males and 15,250 females in US<sup>13</sup>. Human papillomavirus (HPV) infection and tobacco consumption are considered two main causes of head and neck cancer. The HPV-caused HNSCC will gradually diminish when more people receive vaccination<sup>14</sup>. Also, HPV-positive patients have a better prognosis than HPV-negative patients<sup>12</sup>. Thus, tobacco-induced HNSCC is still one of the deadly threats to public health. Generally, the standard of care for HNSCC are surgery, pembrolizumab (programmed death 1 antibodies), pembrolizumab combined with chemotherapy (gemcitabine or cisplatin) and chemo-radiotherapy<sup>15</sup>. Those standards of care will bring ~68% of the 5-year survival rate to HNSCC patients<sup>16</sup>. For survivors, post-therapy quality of life is significantly compromised due to surgery, resulting in difficulty in eating/drinking and speaking<sup>16</sup>. Immunotherapies, like pembrolizumab, are revolutionary breakthroughs in many types of cancer treatments, including HNSCC, by inducing spontaneous and durable remissions. However, the overall response rate of pembrolizumab in HNSCC is ~18%<sup>17</sup>. Therefore, it is necessary to target novel mechanisms to enhance the spontaneous response rate and long-term survival in HNSCC<sup>17</sup>.

Animal models are widely used in cancer therapeutic studies. Wang et al. developed a transplantable model using a 4MOSC1 cell line. This model was developed from a carcinogen-induced tumors which resulted from repeating the application of 4-nitroquinoline-1 oxide to mice through the water supply. This 4MOSC1 cell line shared 93.9% similarity with human cancer signature 4<sup>18</sup>, which is strongly related to tobacco consumption<sup>19</sup>. The similarity is not only in gene signature, but 4MOSC1 also mimics the human HNSCC immune microenvironment, making it a clinically relevant mouse model to study immune therapy in HNSCC. It was demonstrated that this 4MOSC1 model has only limited response to immune checkpoint inhibitor (anti-Pd1); only ~20% of mice reached completed regression upon administration of mouse anti-PD1 immune checkpoint inhibitor, which is similar to human HNSCC response rate toward pembrolizumab<sup>19</sup>.

Major histocompatibility complex class I (MHC-I) molecules with their bound peptides are present in all types of cells in humans and mice. Cellular proteins are cleaved into oligopeptides by the ubiquitin-proteasome pathway, which are then presented by MHC-I molecules to the cell surface. CD8<sup>+</sup> T cells, which can recognize those MHC-I presented peptide antigens, will apply cytotoxicity toward recognized cells. Many cancer cells impair or eliminate this pathway to evade T cell recognition<sup>20</sup>. In many previous studies, MHC-I is a target gene of type I interferon (IFN-I) and interferon-gamma (IFN- $\gamma$ )<sup>21,22</sup>. Demel et al. reported that the SUMOylation inhibitor TAK-981 can robustly synergize with IFN- $\gamma$  to enhance MHC-I expression on multiple blood cancer cells<sup>23</sup>. Because SUMOylation inhibition in myeloid cells, which are abundant in the tumor microenvironment, can stimulate the production of IFN-I and IFN- $\gamma$ , I investigated whether TAK-981 can synergize with IFN-I or IFN- $\gamma$  to increase MHC-I expression on epithelial cancer cells.

T cells play a critical role in antitumor immunity, including its cytotoxicity, immune cell activation, immune cell suppression, and even immune memory function. T cell differentiation starts with naïve T cells' T cell receptors (TCR) recognizing presented antigen peptide by MHC-I or II on antigen presenting cells (APC). Upon TCR-MHC interaction, CD3 protein on T cells initiate downstream intracellular signaling. Besides CD3 protein, other costimulatory and adhesion proteins, such as CD28, 4-1BB, and LFA-1, form large multimolecular complexes to enhance TCR-MHC interaction. With TCR-MHC recognition and amplification of costimulatory factors, these specific antigen-recognized T cells are activated, differentiated, and expanded according to their expression of either CD8 or CD4 and then they will leave APC to actively seek cancer cells that present the same MHC molecules that interact with their TCR. When CD8<sup>+</sup> T cells interact with MHC-I, they will differentiate into cytotoxic T cells that release granzyme B and perforin to kill cancer cells<sup>24</sup>.

T helper cells are subtypes of CD4<sup>+</sup> T cells and can be classified as interleukin-12-driven Th1 cells and interleukin-4-driven Th2 cells, in which Th1 T cells are traditionally considered antitumor factors due to its secretion of IFN- $\gamma$  that polarizes macrophages toward the M1 phenotype<sup>25</sup>. Also, higher amounts of Th1 T cells in tumors were related to better prognosis in various types of tumors<sup>26</sup>. In this study, we assessed the TAK-981 effect on Th1 cells in the tumors, tumor-draining lymph nodes, and spleen via single-cell RNA sequencing or flow cytometry.

After activation and differentiation into either cytotoxic CD8<sup>+</sup> T cells or CD4<sup>+</sup> helper T cells, the T cells with TCR-MHC specific recognition will go over a process called clonal expansion in which antigen-specific T cell populations expand to amplify their function toward eliminating cancer cells. In cancers, chronic stimulation by cancer-related antigens leads to T cell

differentiation into exhaustion due to long-term activation. In exhaustion states, T cells will lose their effector functions, including the secretion of cytokines and tumor cell killing<sup>27</sup>. Recently, researchers found that there is an intermediate state called Stem-like T cells (or, being called by TCF1<sup>+</sup>/PD-1<sup>+</sup>, stem-like exhausted T cells in some literature) between exhausted T cells and activated T cells and plays an important role in the success of immune checkpoint inhibitor<sup>28,29,30,31</sup>. These specific stem-like T cells possess functions like restoring exhausted T cells' killing effects. In this study, I investigate the effects of SUMOylation inhibition on T differentiation in a head and neck tumor microenvironment and tumor-draining lymph nodes.

Before activated T cells become exhausted, some of them will differentiate into memory T cells, including stem-like memory T cells (T<sub>SCM</sub>), central memory T cells (T<sub>CM</sub>), and effector memory T cells (T<sub>EM</sub>), which play an important role in antitumor immunity<sup>32</sup>. Overall, these memory T cells have less stringent requirements for the second activation toward cancer cells. The T<sub>CM</sub> cells, compared to T<sub>EM</sub> cells, produce higher levels of cytokines, have stronger cytotoxic activity *in vitro*, and last longer than T<sub>EM</sub> cells *in vivo*<sup>33,34,35</sup>. In studies of melanoma, head and neck cancer, and non-small cell lung cancer, a higher T<sub>CM</sub> population also showed a positive correlation with better clinical outcomes<sup>37,36</sup>. Considering the importance of memory T cells in antitumor effect, I analyzed the T<sub>CM</sub> and T<sub>EM</sub> cell populations in the tumor, tumor-draining lymph nodes, and spleen of 4MOSC1 head and neck cancer-bearing mice via flow cytometry.

Regulatory T cells (Treg) are differentiated from CD4<sup>+</sup> T cells with upregulation of forkhead box P3 (FOXP3) transcription factor and interleukin 2 (IL-2) receptors. With higher IL-2 receptor surface expression, Treg competes effectively with CD8<sup>+</sup> T cells for IL-2, a cytokine that leads to T cells' expansion to suppress immune response<sup>37</sup>. The regulatory, or suppressive,

function of Treg is critical to prevent unhealthy strong immune responses. In healthy adult mice, the elimination of Treg cells caused the death of mice due to the overreacted immune system under diphtheria toxin condition<sup>38</sup>. However, in the tumor microenvironment, a higher Treg population showed a correlation with poor prognosis<sup>39</sup>. Wang and colleagues showed that depletion of Treg in 4MOSC1 tumor-bearing mice resulted in slower tumor growth<sup>19</sup>. In my study, I investigated the population of Treg in the tumor microenvironment and tumor-draining lymph node via single-cell RNA sequencing and flow cytometry.

## Chapter 2 METHODS and MATERIALS

### 2.1 Cell line and Cell culture

The 4MOSC1 and MOC1 mouse head and neck squamous cell carcinoma cell lines were kindly given by J. Silvio Gutkind's lab at the Moores Cancer Center. 4MOSC1 cells were cultured in Defined Keratinocyte-SFM medium with mouse epidermal growth factor (5 ng/mL), cholera toxin (0.05 nM), and 1% antibiotic/antimycotic (Anti-anti) solution in a collagen pre-coated plate. 0.4 mg/mL of collagen with 1% of acetic acid were used to coat the cell culture plate for 15-20 minutes, and the coated cell culture plates were washed with phosphate-buffered saline twice before seeding cells. The MOC1 murine HNSCC cell line was cultured in 62.6% HyClone Iscove's Modified Dulbecco's Medium (sh30228.02, cytiva) with 31.3% hams nutrient mixture (sh30026.01 cytiva), 5 % heat-inactive fetal bovine serum, 1% Anti-anti, 5 mg insulin (I6634-50mg, Sigma Aldrich), 40 ug hydrocortisone (H0135-1mg, Sigma Aldrich) and 5 ug human recombinant epidermal growth factor (01-107, EMD Millipore).

### 2.2 Orthotopic tumor implantation

Prior to 4MOSC1 tumor cell implantation, the cells in the cultured dish were washed with phosphate-buffered saline once and loosened by 1 mL of 0.25% trypsin. The trypsin digestion process was terminated by adding 10 mL of 10% fetal bovine serum and 1% antibiotic/antimycotic Dulbecco's Modified Eagle Medium. The cells then were resuspended in the cultured medium at 500,000 per 40 microliters; the cells will only be used for tumor implantation once their viability is >85% via Countess 3 Automated Cell Counter (ThermoFisher Scientific). For tongue, 4MOSC1 tumor implantation, 500,000 (in 40  $\mu$ L cell-resuspended culture medium) 4MOSC1 cells were injected into the tongue of female C57BL/6 mice (6-8

weeks of age from the Jackson Laboratory) under isoflurane anesthesia condition. Prior to MOC1 tumor cell implantation, the plates were washed with PBS and changed media 2-6 hours before harvest. Right before tumor inoculation, the plates with cells were washed with PBS once and treated with 5 mL 0.25% trypsin. After around 10 minutes, the plates were observed to make sure cells were rounded and floating. The trypsin digestion process was terminated by adding 10 mL MOC1 cultured media. The cells were then spined down and resuspended in PBS. This spin-down and resuspend procedure were repeated once to eliminate residue MOC1 culture media, and the cells were resuspended in PBS at a final density of 1 million cells per 16.66 uL. For each 16.66 uL MOC1-PBS solution, 33.3 uL of cultrex basement membrane extract (3432-010-01, R&D system) were added. For tongue MOC1 tumor implantation, 1 million (in 50 ul of 1:2 PBS and cultrex basement membrane extract mixture) MOC1 cells were injected into the tongue of female C57BL/6 mice (6-8 weeks of age from the Jackson Laboratory) under isoflurane anesthesia condition. Following tumor implantation, 5 consecutive days of visiting were done with a well record. On day 5, after tumor inoculation, soft food was supplied to help the mice with the tongue tumor swallow. The mice were sacrificed at the indicated time points or the endpoint, which was determined when the mice's tumor was > 8 mm in greatest diameter or ulcerated.

### **2.3 Tongue tumor size measurement**

After 5 days of tumor implantation, mice were observed, and tongue tumors were measured twice a week. During the tongue tumor measurement, the mice were first anesthetized with an isoflurane anesthesia machine (VetEquip, #901807SO). Then, the unconscious mouse was placed under a nose cone, which provided a constant low dose of isoflurane-oxygen mixed

gas. The mouse tongue was brought out by a tweezer and the tumor was measured by dental castroviejo caliper.

#### **2.4 *In vivo* antibodies and small molecular drug dosing**

SUMOylation inhibitor TAK-981 (CT-TAK981) was ordered from Chemitec and first diluted in dimethyl sulfoxide (DMSO) at 120 mg/mL. The first-diluted TAK-981 then further diluted with 5% dextrose, 20% kolliphore EL water solution (vehicle solution). The mouse would receive 15 mg of TAK-981 per kilogram bodyweight (A 20-gram mouse will receive 0.3 mg of TAK-981). TAK-981 dosing was applied twice a week through intraperitoneal injection. The anti-mouse programmed death-1 (anti-PD-1) antibody (BP0146) was ordered from BioxCell and was diluted in BioxCell InVivoPure pH 7.0 Dilution Buffer (IP0070). Every mouse under anti-PD-1 treatment will receive 10 mg of anti-PD-1 per kilogram bodyweight (A 20-gram mouse will receive 0.2 mg of anti-PD-1) three times a week through intraperitoneal injection<sup>18</sup>.

#### **2.5 Mouse sacrifice and cell collection from mouse**

For flow cytometry and single-cell RNA-seq, the tumor, lymphatic, spleen, or peripheral blood mononuclear cells (PBMC) were collected from 4MOSC1-bearing mice at day 15 after tumor implantation. The tongue tumors were resected at day 15 and cut into pieces at 3-4 mm in size. Tumor pieces were then put into a Miltenyi Mouse Tumor Dissociation kit (130-096-730) and ground by gentleMACS™ Dissociator according to the manufacturer's recommendations for tumor dissociation. After tumor dissociation, the tumor tissue was digested, and the digested tissues were passed through 70 µm to acquire single-cell suspension. Then, red blood cells in tumor single-cell suspension were lysed by ACK Lysing Buffer (Gibco A1049201) via

submerging the single-cell suspension solution in ACK lysing buffer for 2 minutes at room temperature. The red blood cell-free single-cell suspension solution will then be subjected to a downstream analysis experiment. After tumor training, lymph nodes were collected from mice<sup>44</sup>, and the lymph nodes were ground on a 70  $\mu\text{m}$  strainer. The cells that pass the strainer will be collected for future study. Spleens were collected from mice and placed on a 70  $\mu\text{m}$  strainer for grinding. The post-strainer spleen cells were then placed in ACK Lysis Buffer to remove red blood cells. After red blood cell removal, the spleen cells were used for downstream analysis. After collecting mouse blood through heart punctation with 20  $\mu\text{L}$  ethylenediaminetetraacetic acid (EDTA), the blood was layered on the same volume of Lymphoprep (STEMCELL, 07851) buffer in a tube. This 2-layer solution was then centrifuged at room temperature at 800 x g for 20 minutes. Then, the proper layer of PBMC was collected and ready for downstream analysis.

## **2.6 Flow Cytometry Sample Acquire and Analysis**

Single-cell suspension solution from Tumor, spleen, or lymph node and isolated PBMC were washed with cell staining buffer (2% FBS, 5mM EDTA, and Dulbecco's Phosphate-Buffered Saline). Then, the cell suspensions were first stained with Zombie yellow (Biolegend, 423104) (1:100) at room temperature for 15 minutes, protected from light to identify dead cells—the cells' suspension solution after Zombie yellow staining was then washed three times with cell staining buffer. Cell surface staining was processed for 30 minutes at 4 °C protected from light with the following anti-mouse antibodies: CD45 (Cytex, 30-F11), CD3 (BD biosciences, 563565), Viability blue Live/Dead (ThermoFisher, L23105), CD8 (ThermoFisher, 368-0081-82), CD4 (Bio-Rad, MCA2691SBUV605), CD69 (Bio-Legend, 104530), CD62L

(Bio-Legend, 104450), CD44 (ThermoFisher, 365-044-82), CD127 (Bio-Legend, 158214), CD25 (Bio-Legend, 102048), TIM3 (Bio-Legend, 134010), PD1 (BD biosciences, 568603), CD11c (Bio-Legend, 117368), CD103 (BD biosciences, 566118), TIGIT (BD biosciences, 565270). After cell surface staining, the cells were first washed three times with cell staining buffer and then fixed at 4% formaldehyde solution at 4 °C for 30 minutes, protected from light. A wash process was performed after fixation. If intracellular staining is needed, the post-surface-staining cells were permeabilized and fixed with Foxp3/Transcription Factor Staining Buffer Set (ThermoFisher, 00-5523-00) according to the manufacturer's recommended procedures. Anti-mouse intracellular antibodies were TCF1/7 (Cell signaling, 14456S), FOXP3 (ThermoFisher, MA5-18160), Tbet (BD biosciences, 568167), TOX (BD biosciences, 570193). Post-intracellular staining cells were washed twice with permeabilization buffer diluted according to the manufacturer's manual. Samples were acquired using NovoCyte Advanteon Flow Cytometer System 1-3 Lasers or Cytex Aurora 5L full spectrum Cytometry, and FlowJo TM v10 Software analyzed the acquired data.

## **2.7 Single-cell RNA sequencing sample preparation and data analysis**

In both the control and SUMOi treated groups, two mice's tumor single-cell suspension solutions of the same groups were evenly combined and labeled with either the control or SUMOi group. For single-cell library construction, the mixed single-cell suspension solution from tumors was subjected to a dead cell removal kit (Miltenyi Biotec, 130-090-101). The cells' viability was determined by Countess 3 automated Cell counter (ThermoFisher Scientific), and the dead cell removal procedure was repeated if the cells' viability was lower than 90%. Then, 10,000 cells from each group were used for library construction. The 10,000 single-cell

suspensions were first used for RNA extraction, reverse transcription, and polymerase chain reaction (PCR) with Chromium Next GEM Single Cell 3 HT Reagen Kits v3.1. At this step, a barcode, a unique molecular identifier (UMI), and a poly(dT) primer were attached to each RNA fragment to identify reads that originate from the same cell, removing repeated DNA duplicates after the PCR step and initiating reverse transcription with PCR. Then, the barcoded UMI and poly(dT) primer attached were selected for cDNA amplification for the library. In the library construction step, the cDNA samples from each group were first subjected to enzymatic fragmentation to cut the long cDNA into pieces that were suitable for sequencing. And adaptor oligos were attached to those cDNA pieces. Excess adaptor oligos were removed with magnet beads from samples. Then, sample indexes were attached to the adaptor oligos attached cDNA pieces. Size selections were performed on both adaptor oligos and sample index attached samples, in which excess sample index fragments and cDNA fragments that are not suitable for sequencing will be removed. Quality control was done with an Agilent Bioanalyzer High Sensitivity chip by a UCSD IGM Genomics Center staff. Then, the library was sequenced on an Illumina NovaSeq 6000 S4 at 200M reads per sample.

Data analysis was performed in R with Seurat<sup>41</sup>.

## **2.8 Cell lysis and western blot**

TAK-981 treated or untreated cells in 6 wells plate were lysed with 200  $\mu$ L 25% 4x Laemmli SDS non-reducing buffer, 5%  $\beta$ -mercaptoethanol, and 70% ultra-pure water. Right after adding the lysis buffer, the plate with cells was scraped and collected into tubes. Then, cell lysates were sonicated at 20 MHz and 10 seconds four times; a 30-second interval was held between each sonication, and the samples were kept on ice during 30-second intervals. After four

times of sonication, DNA degradation was determined by the viscosity of the sample and the non-viscous samples were boiled at 99 °C for 30 minutes to denature the protein. Denatured protein samples were loaded to 10-wells NuPAGE™ 4 to 12 %, Bis-Tris, 1.0-1.5 mm, Mini Protein Gels (Invitrogen, NP0321BOX). Then, proteins were transferred from the protein gel to the nitrocellulose membrane (Invitrogen, Nitrocellulose/Filter Paper Sandwich, 0.2 µm, 8.3 x 7.3 cm) in a cold room. The nitrocellulose membranes with transferred protein were blocked by 5% non-fat milk for 1 hour at room temperature. Primary antibodies SUMO2/3 (cell signaling, 4971) and GAPDH (Invitrogen, MA5-15738) were applied to membranes in a cold room via overnight incubation. On the second day, the primary antibodies attached to the membranes were collected from the cold room and washed for 15 minutes with Tris-Buffered Saline with Tween 20 three times at room temperature. Then, the membranes were incubated with fluorescent secondary antibodies (1:10000) for 45 minutes at room temperature. Secondary antibodies bind membranes were washed 15 minutes with Tris-Buffered Saline with Tween 20 for three times at room temperature and imaged by the Odyssey detection system (LICOR)

## **2.9 Statistical analysis**

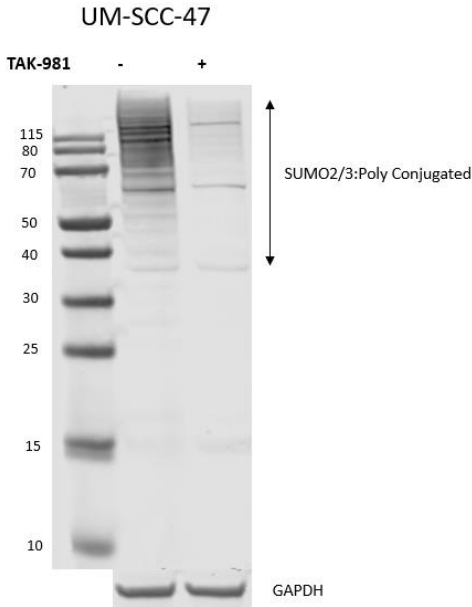
The statistical analysis of data was calculated using GraphPad Prism for Windows. The significance of flow cytometry data between the experimental and control groups was measured by independent t-test, one or two-way ANOVA with multiple comparisons. The significance of the survival test between the experimental and control groups was measured by the Kaplan-Meier method and log-rank tests. In the figures, the \* represents  $P < 0.05$ , the \*\* represents  $P < 0.01$ , and the \*\*\* represents  $P < 0.001$ .

## Chapter 3 RESULTS

### **3.1 SUMOylation inhibition by TAK-981 in human and murine HNSCC cell line**

Before studying the effect of SUMOylation inhibition on mouse tumor models *in vivo*, we validated that TAK-981 can inhibit SUMOylation in both human and mouse HNSCC cell lines *in vitro*. Human UM-SCC-47 and murine MOC1 HNSCC cells were treated with 100 nM TAK-981 for 24 hours; then the extracted protein was used to perform western blot for SUMO2/3 protein (Figure 3-1 (A), (B)). Under 100 nM TAK-981 treatment, less SUMO2/3:poly protein conjugation was detected in both cell lines, which indicated that TAK-981 effectively inhibited SUMOylation activity in these cancer cells.

A).



B).

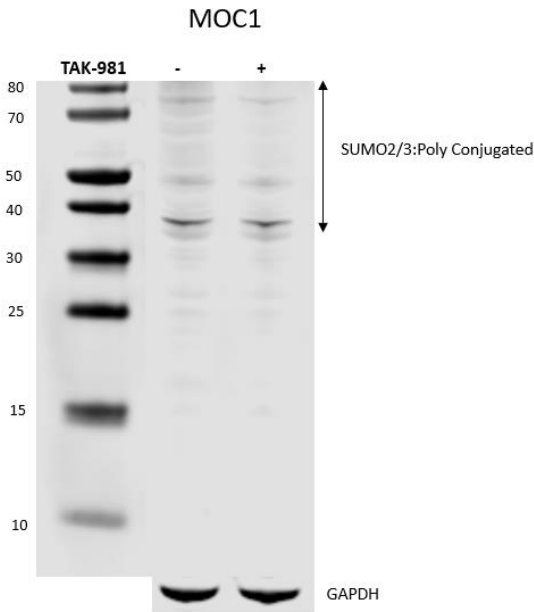


Figure 3-1: Western blot for SUMOylation in human and murine HNSCC cell line. (A). Western blot of UM-SCC47 cells extracted protein for SUMO 2/3 protein. Lane 1: protein ladder. Lane 2: SUMO2/3 western blot for UM-SCC47 extracted protein with vehicle control. Lane 3: SUMO2/3 western blot for UM-SCC47 extracted protein with 100 nM TAK-981 treatment for 24 hours. (B). Western blot of MOC1 cells extracted protein for SUMO 2/3 protein. Lane 1: protein ladder. Lane 2: SUMO2/3 western blot for MOC1 extracted protein with vehicle control. Lane 3: SUMO2/3 western blot for MOC1 extracted protein with 100 nM TAK-981

### **3.2 SUMOylation inhibitor enhanced survivals in 4MOSC1 HNSCC tumor-bearing mice, and responding mice showed immunological memory**

To establish a tumor model, we implanted 500,000 murine HNSCC 4MOSC1 cells on mouse tongues. When tumors formed, mice were treated with TAK-981 by intravenous (IV) injection. The SUMOylation inhibitor significantly increased mouse survival (Figure 3-2 (A)). Since the tongue tumors are visible and accessible, tumor volume measurement was carried out. In the TAK-981 mono-therapy group, the median survival was significantly extended compared with the control group. Also, the tumor in one mouse completely regressed in the TAK-981 treated group (Figure 3-2 (A)). An endpoint of the experiment is ulcer formation in tumors. TAK-981 treatment slowed down ulcer formation in the tongue tumors. The mouse that TAK-981 cured was injected with the same tumor cells 49 days after the complete regression. A naïve mouse was also injected with the same tumor cells as a control group. The previously treated mouse quickly rejected the tumor from the second implantation of 4MOSC1, while the control mouse developed a tumor that developed an ulcer on day 11, reaching the experimental endpoint (Figure 3-2 (D)).

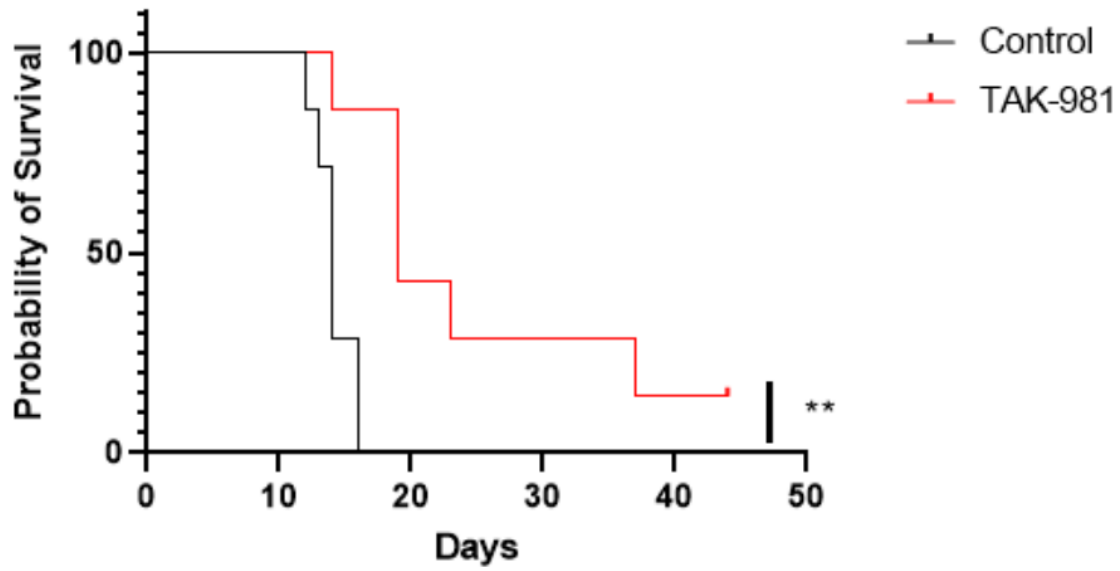
A).



Figure 3-2. Evaluation of the effect of SUMOylation inhibition in the 4MOSC1 murine model. (A). 4MOSC1 tumor on mouse tongue (B). Survival rates of the control group (treated with vehicle) and the TAK-981-treated group. Mice were injected with 500,000 4MOSC1 cells on their tongues. (C). Tumor volume vs. Days plot from (A). (D). Tumor volume vs. Days plot of the tumor rechallenge experiment on a naïve mouse and the cured mouse shown in (B).

Figure 3-2. continued

B).



C).

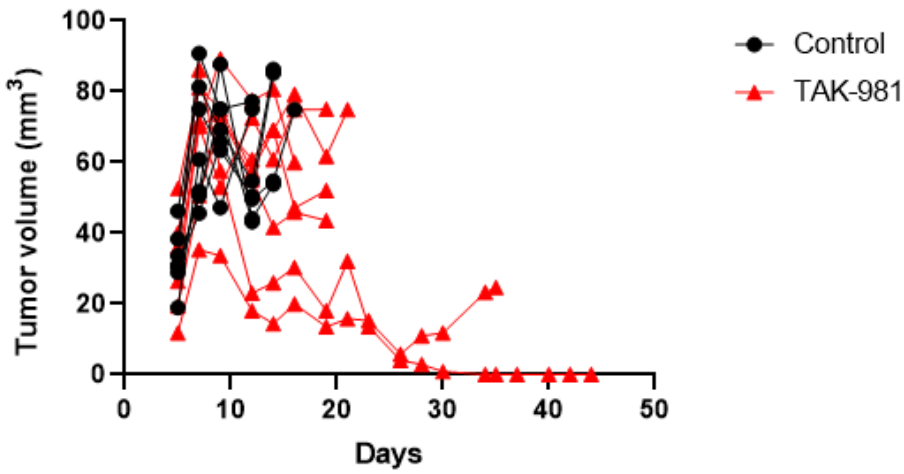
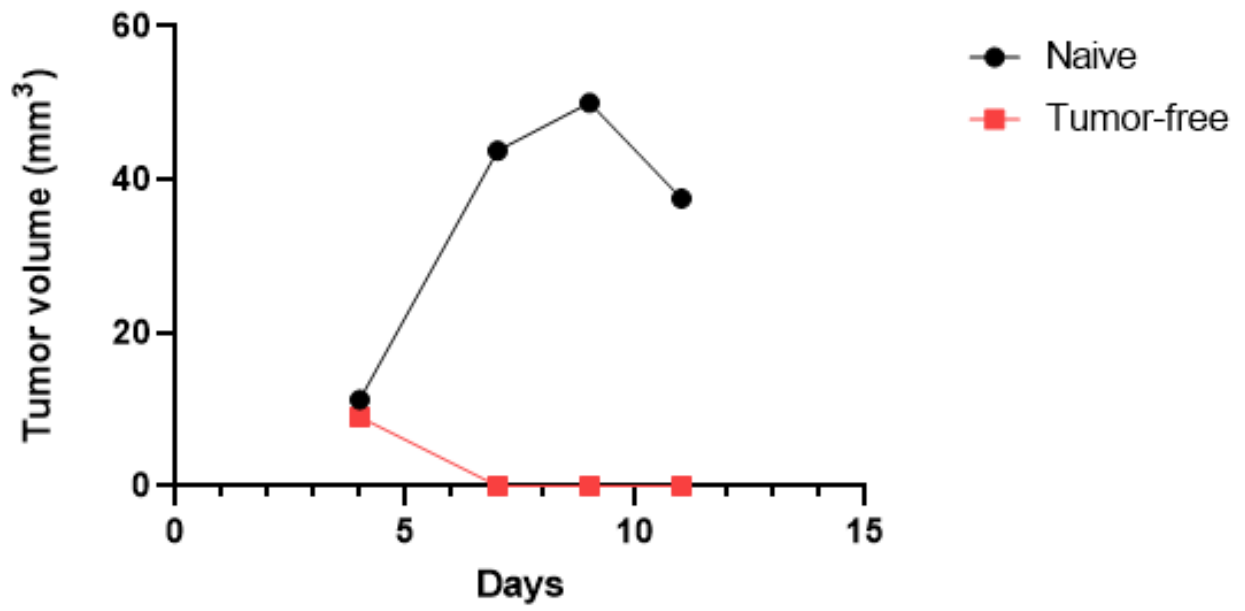


Figure 3-2. continued

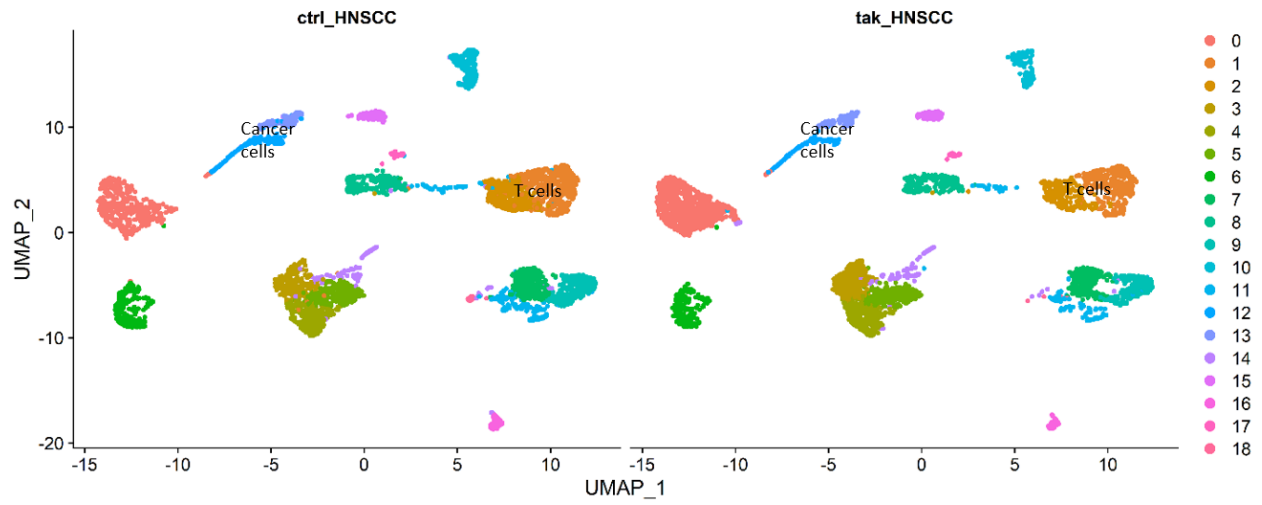
D).



### **3.3. Investigation of the effect of SUMOylation inhibition on the murine HNSCC tumor microenvironment using single-cell transcriptomics**

To understand why the SUMOylation inhibitor was able to enhance survival of 4MOSC1-bearing mice, we conducted single-cell RNA sequencing analysis on tumor-dissociated single cell suspension. In 4MOSC1-bearing mice, the tumors from both the vehicle control group and TAK-981 treated group were collected at day 15 after tumor inoculation (n=2 in each group). The gene library was constructed according to Chromium Next GEM single Cell 3' HT v3.1 (dual index) protocol from 10x Genomics. The library was then sequenced. For downstream analysis, we first used hierarchical clustering to separate the cells into 18 different cell types. Due to our finding of immunological memory formation in the rechallenge experiment (Fig. 3-2), we further analyzed T cell-related processes. T cells cluster 1 and 2 in Figure 3-3 (A) and (B) that express *Cd3e*, *Cd8a*, and *Cd4*.

A).



B).

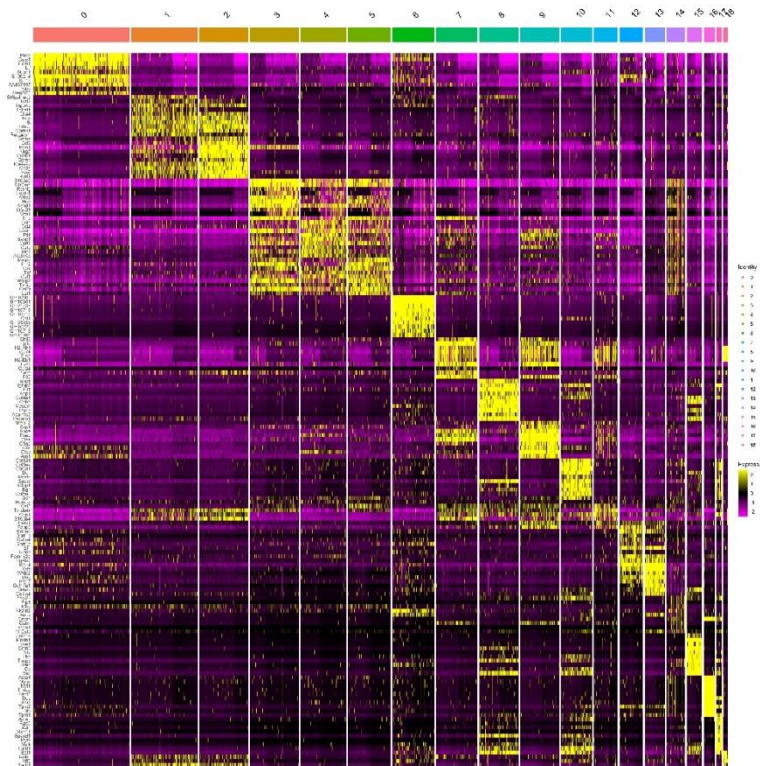


Figure 3-3. Single cell transcriptomic analysis of the 4MOSC1 tumors. (A) UMAP of 4MOSC1 tumor tissue single-cell RNA-seq. ctrl\_HNSCC: vehicle control group. tak\_HNSCC: TAK-981 treated group. (B) heatmap of hierarch clustering on 4MOSC1 tumor tissue.

### 3.4 Single-cell transcriptomics revealed that SUMOylation inhibition impacts T cell differentiation and activation

We further sub-clustered *Cd3e* expressing cells (T cells) into 11 clusters to define T cell subsets according to literature: CD8<sup>+</sup>CD11c<sup>+</sup> T cells (*Cd8b1*, *Itgax*)<sup>42</sup>, helper 2 T cells (*Cd4*, *Gata3*)<sup>43</sup>, effector T cells (*Cd8a*, *Gzmb*, *Tbx21*, *Ifng*, *Tnf*)<sup>44</sup>, stem-like T cells (*Tcf1*, *Tox*, *Sell*, *Ccr7*)<sup>28</sup>, regulatory T cells (*Cd4*, *Foxp3*, *Gzmb*)<sup>45</sup>, terminal exhausted CD8<sup>+</sup> T cells (*Cd8a*, *Foxp3*, *Gzmb*, *Havcr2*, *Lag3*)<sup>46</sup>, helper 1 T cells (*Cd4*, *Tbx21*, *Ifng*)<sup>44</sup>, NK T cells (*Cd3e*, *Klrb1c*)<sup>47</sup> and three unknown groups that are of small population (Figure 3-4 (A), (B)). In Figure 3-4 (C), a proportional test of T cell subsets was performed, and we found fewer CD8<sup>+</sup>CD11c<sup>+</sup> T cells in the TAK-981 treated tumors. CD11c is expressed at levels on most dendritic cells, but can also be found on monocytes, macrophages, neutrophils, and some B cells. CD11c, also known as integrin alpha-X, mediates cell-cell interactions<sup>48,49</sup>. The functions of CD11c expressing CD8<sup>+</sup> T cells in anti-tumor immunity are unclear. One report suggested that they have CD4<sup>+</sup> T cell depletion function<sup>42</sup>. There were no significant changes in the populations of effector T cells, stem-like T cells, or regulatory T cells. However, we found that the terminal exhausted T cell population was decreased in the TAK-981 treated group. In addition, the effector T cells in TAK-981 treated tumors have increased expression of IFN- $\gamma$  and tumor necrosis factor alpha (TNF $\alpha$ ) compared with effector T cells in the vehicle group. This data suggests that TAK-981 treatment increased the cytotoxic function of effector T cells. Taken together, these findings indicate that SUMOylation inhibition reduced T cell exhaustion and enhanced T cell activation and effector function.

A).

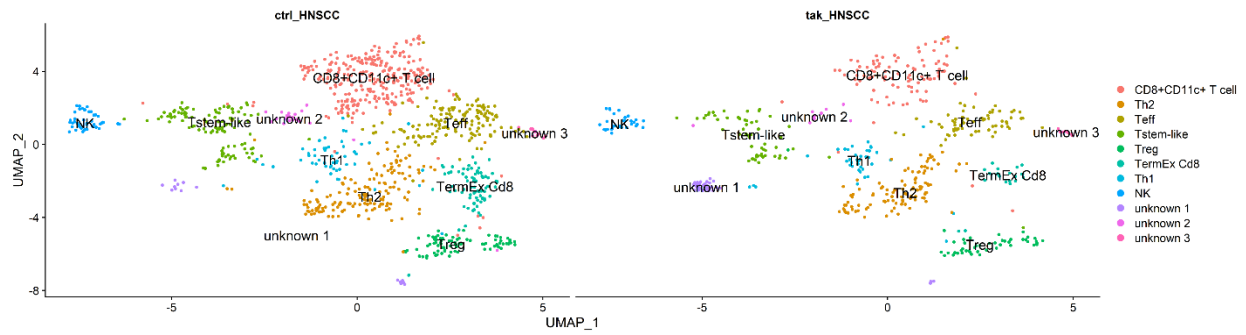


Figure 3-4. Single cell transcriptomic analysis of T cells. (A). UMAP of T cell subsets. ctrl\_HNSCC: control group, tak\_HNSCC: TAK-981 treated group. (B). Heatmap of T cell subset clusters in CD3<sup>+</sup> cells. (C). Proportional test of each subset of T cells in CD3<sup>+</sup> cells, ctrl: control group, tak: TAK-981 treated group. (D). The violin plot shows the differences in IFN- $\gamma$ , TNF $\alpha$ , and granzyme B expression levels in effector T cells. Teff\_tak: effector T cells in TAK-981 treated group. Teff\_ctrl: effector T cells in the control group. The numbers above the plot represent the adjusted P value.

Figure 3-4. continued

B).

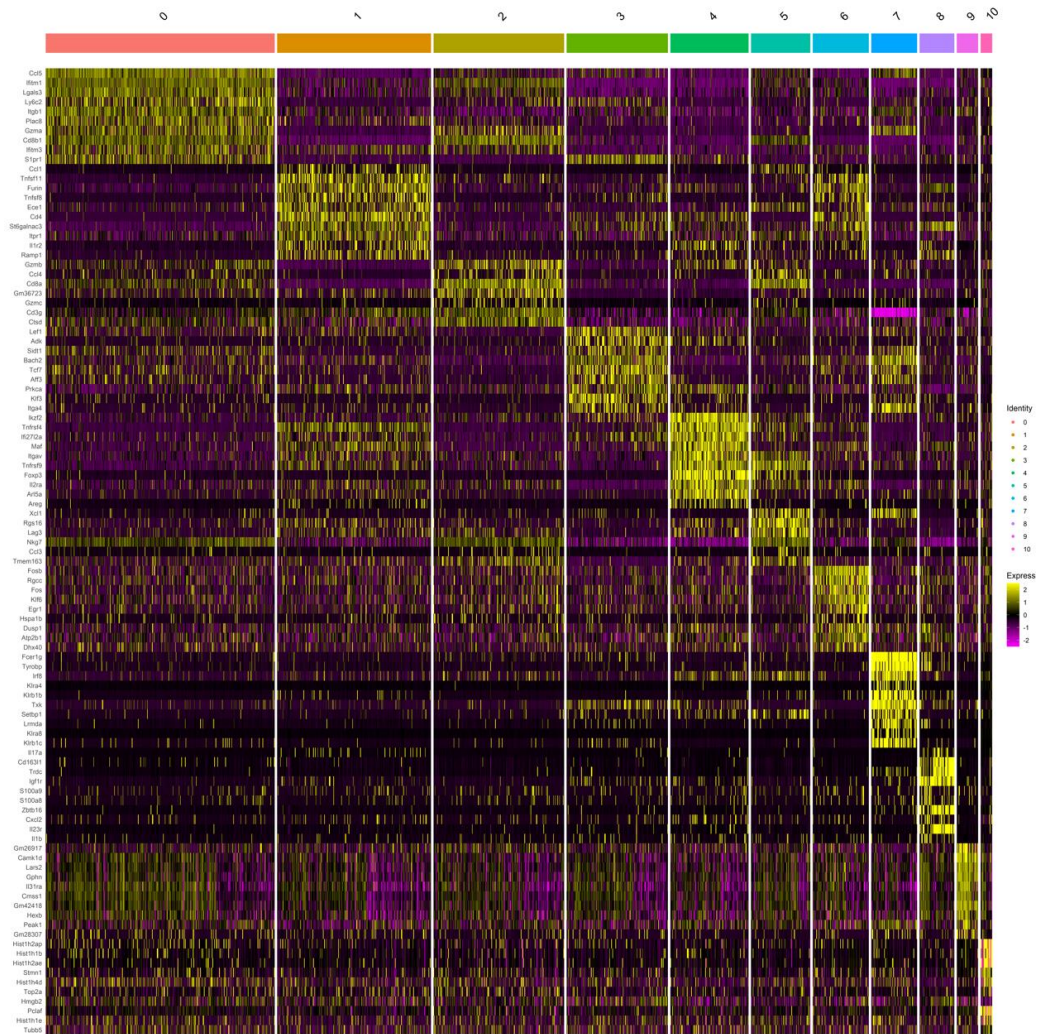


Figure 3-4. continued

C).

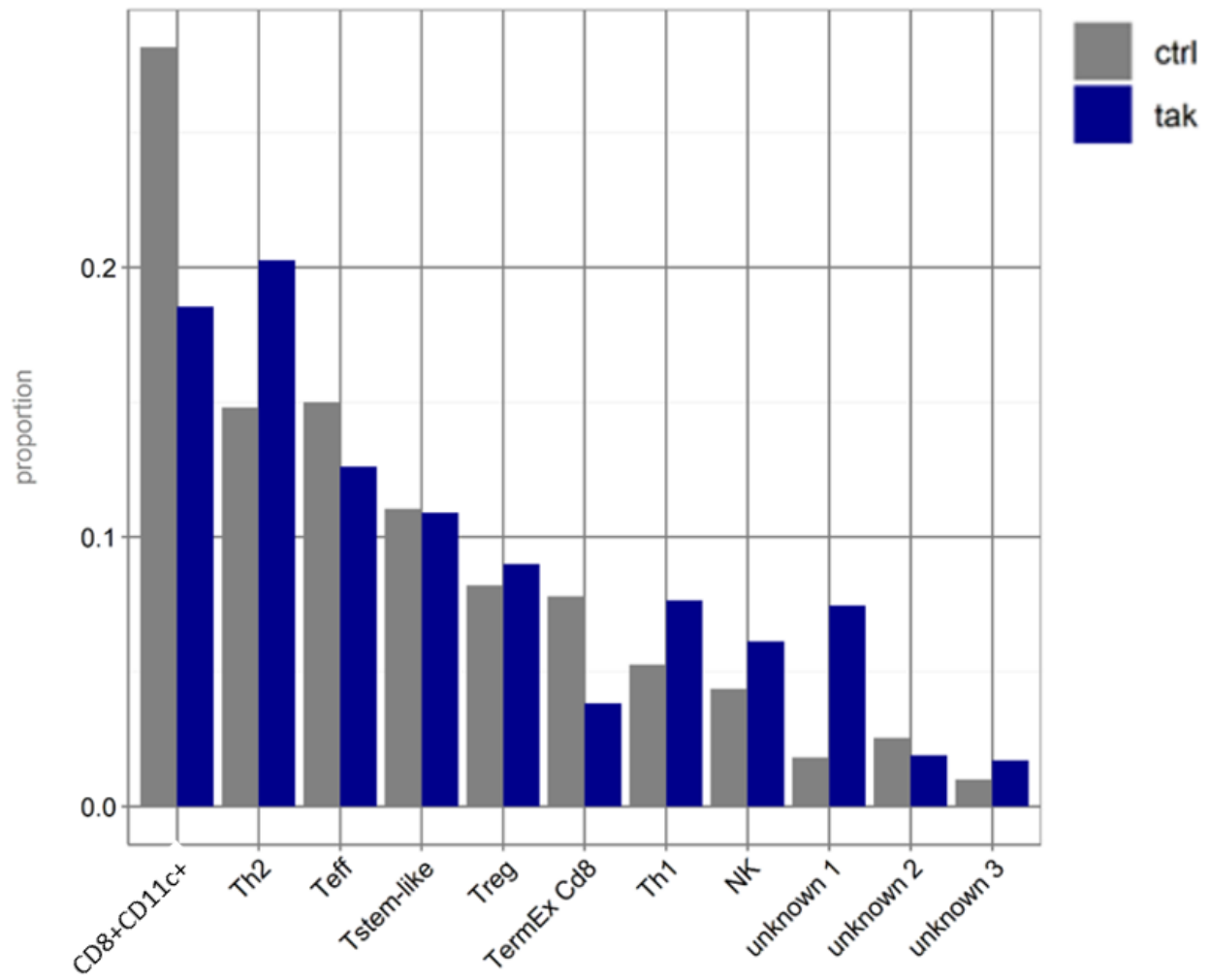
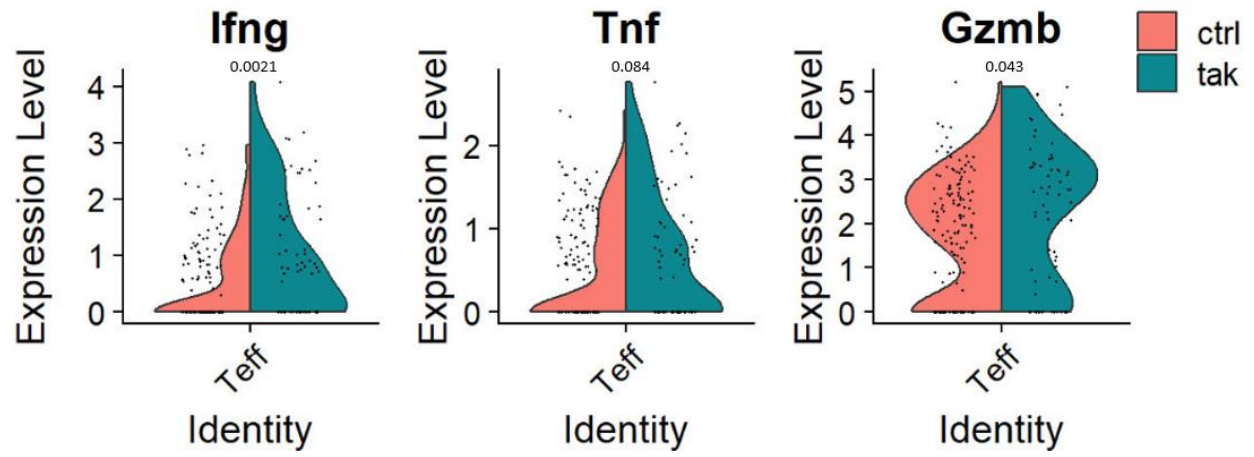


Figure 3-4. continued

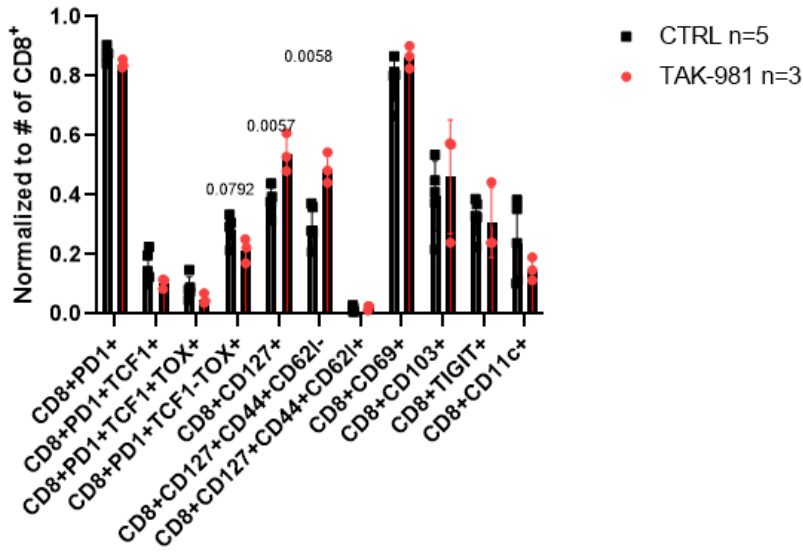
D).



### **3.5. TAK-981 treatment increased effector memory T cell population in tumors of the HNSCC mouse model as shown by flow cytometry**

To validate our finding from single-cell transcriptomics, I carried out flow cytometry on collected tumor tissue from HNSCC-bearing mice. I found that both CD4<sup>+</sup> and CD8<sup>+</sup> effector memory T cells (CD127<sup>+</sup>CD44<sup>+</sup>CD62L<sup>-</sup>)<sup>50,51</sup> are significantly increased in the TAK-981 treated group. Increased expression of effector marker CD44 is consistent with findings from single cell transcriptomics that TAK-981 treatment increased T cell effector function (Figure 3-5 (A) and (B)). The expression of CD127, the receptor for IL7, is associated with T cell self-renewal potential<sup>52</sup>. Therefore, SUMOylation inhibition, increased self-renewal potential of T cells. In addition, terminally exhausted T cells (CD8<sup>+</sup>PD1<sup>+</sup>TCF<sup>-</sup>TOX<sup>+</sup>)<sup>53</sup> were reduced in the TAK-981 treated group (Figure 3-5 (A)). Consistent with single-cell data, we also observed a decreasing trend in CD8<sup>+</sup>CD11c<sup>+</sup> T cells that remains further investigated. Taken together, these findings suggest that SUMOylation inhibition increased T cell activation and the expression of a surface receptor (CD127) known to enhance memory formation and reduced T cell exhaustion.

A).



B).

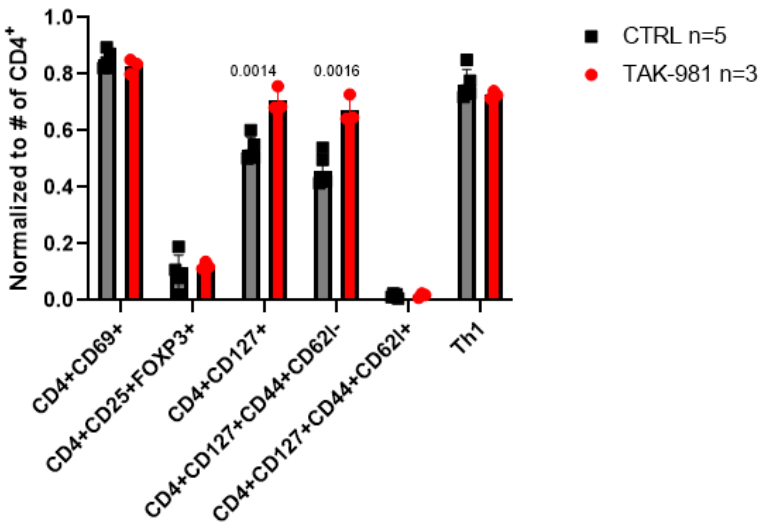


Figure 3-5. Flow cytometry analysis of 4MOSC1 tumors. (A). CD8<sup>+</sup>PD1<sup>+</sup> T cells, CD8<sup>+</sup>PD1<sup>+</sup>TCF1<sup>+</sup> T cells, CD8<sup>+</sup>PD1<sup>+</sup>TCF1<sup>+</sup>TOX<sup>+</sup> T cells, CD8<sup>+</sup>PD1<sup>+</sup>TCF1<sup>+</sup>TOX<sup>+</sup> T cells, CD8<sup>+</sup>PD1<sup>+</sup>TCF1<sup>-</sup>TOX<sup>+</sup> T cells, CD8<sup>+</sup>CD127<sup>+</sup> T cells, CD8<sup>+</sup>CD127<sup>+</sup>CD44<sup>+</sup>CD62L<sup>-</sup> T<sub>EM</sub> cells, CD8<sup>+</sup>CD127<sup>+</sup>CD44<sup>+</sup>CD62L<sup>+</sup> T<sub>CM</sub> cells, CD8<sup>+</sup>CD69<sup>+</sup> T cells, CD8<sup>+</sup>CD103<sup>+</sup> T cells, CD8<sup>+</sup>TIGIT<sup>+</sup> T cells and CD8<sup>+</sup>CD11c<sup>+</sup> T cells population in 4MOSC1 bearing mice tumor. CTRL: vehicle-treated, TAK-981: TAK-981 treated. The numbers above the bars represent the P value. (B). CD4<sup>+</sup>CD69<sup>+</sup> T cells, CD4<sup>+</sup>CD25<sup>+</sup>FOXP3<sup>+</sup> T cells, CD4<sup>+</sup>CD127<sup>+</sup> T cells, CD4<sup>+</sup>CD127<sup>+</sup>CD44<sup>+</sup>CD62L<sup>-</sup> T<sub>EM</sub> cells, CD4<sup>+</sup>CD127<sup>+</sup>CD44<sup>+</sup>CD62L<sup>+</sup> T<sub>CM</sub> cells and CD4<sup>+</sup>Tbet<sup>+</sup> Th1 cells population in 4MOSC1 bearing mice tumor. CTRL: vehicle-treated, TAK-981: TAK-981 treated. The numbers above the bars represent the P value.

### **3.6 SUMOylation inhibition synergized with IFN- $\gamma$ and IFN- $\alpha$ to upregulate MHC-I expression on murine HNSCC cell surface**

CD8 T cells recognize and kill tumor cells through binding to MHC-I that present tumor-specific antigens (neoantigens). Thus, a mechanism for tumor cells to escape from anti-tumor immunity is through the downregulation of surface MHC-I expression<sup>54</sup>. Analysis of single cell transcriptomics showed an increase of MHC-I genes in TAK-981 treated tumor cells. In the UMAP plot of all cell types in a tumor (Figure 3-3 (A)), clusters 12 and 13 expressed high *Epcam* levels, an epithelial cell marker, and the highest *Krt5*, a marker of 4MOSC1 tumor cells<sup>19</sup>. Therefore, these two groups are 4MOSC1 cancer cells. We compared MHC-I (*H2-K1*, *H2-Q6*, *H2-Q4*, *H2-D1*, *H2-Q7*, and *H2-Q10*) expression levels between SUMOylation inhibition and control groups (Figure 3-6 (A)). The expression of *H2-K1* and *H2-D1*, which are MHC-Ia genes widely expressed, was upregulated in the TAK-981 treated group compared with the control group *in vivo*.

Then, we tested whether H2-K1 and H2-D1 protein levels on tumor cell surface increased and determined whether SUMOylation inhibition of tumor cells has a direct effect in increasing their upregulation by treating the tumor cells with TAK-981 *in vitro* and probing these MHC-I proteins via flow cytometry. Besides TAK-981, we also examined the effect of IFN- $\gamma$  and type I IFN due to their well-known function of increasing MHC-I expression and that inhibiting SUMOylation in T and myeloid cells in the tumor microenvironment could increase the expression of IFN- $\gamma$  and IFN- $\beta$  (an IFN binding to the same receptor as IFN- $\alpha$ ). Treatment of the cancer cells with TAK-981 alone did not significantly increase these MHC-I. As described previously in the literature<sup>21,22</sup>, IFN- $\gamma$  and IFN- $\alpha$  were able to upregulate MHC-I expression on the 4MOSC1 cell surface. Interestingly, TAK-981 enhanced IFN- $\gamma$  or IFN- $\alpha$ -induced MHC-I

expression on 4MOSC1 cells (Figure 3-6 (B), (C), (D) and (E)). These data indicate that SUMOylation inhibition increases the expression of MHC-I on cancer cells through stromal cells in the tumor microenvironment, and the direct inhibition of TAK-981 on tumor cells further enhanced the effects mediated by the stroma cells.

A).

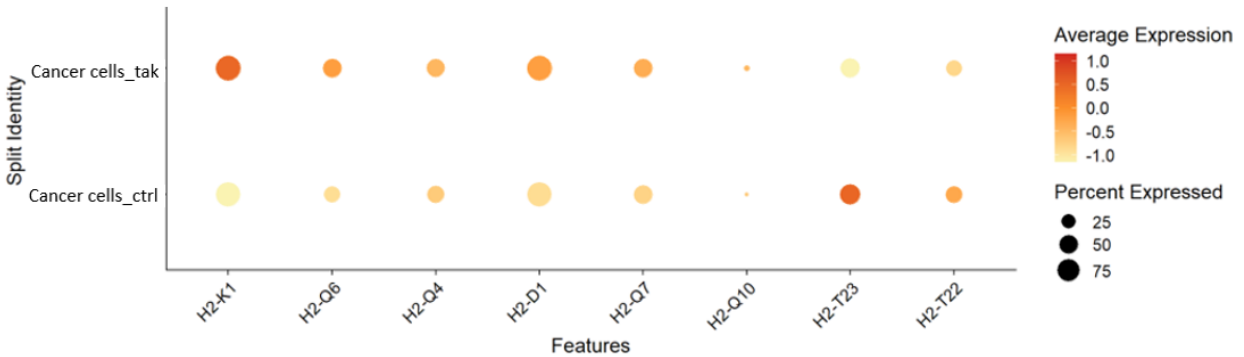
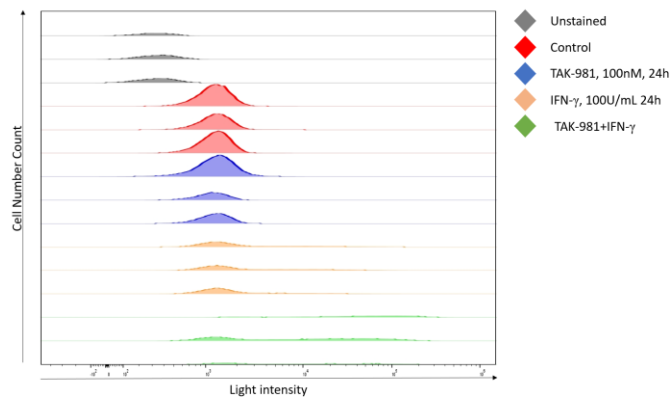


Figure 3-6. Regulation of MHC-I expression on tumor cells by SUMOylation inhibition. (A). MHC-I molecule gene expression level on cancer cell from the single cell RNA-Seq data. Cancer cells\_tak: cancer cells cluster from the TAK-981 treated group. Cancer cells\_ctrl: cancer cells cluster from vehicle treated group. (B). Fluorescent median intensity peak chart of MHC-I levels in flow cytometry. The unstained control group is cells mixed from all groups without anti-mouse MHC-I antibodies, The Control group was treated by DMSO, TAK-981 group was treated by TAK-981 at 100 nM for 24 hours, IFN- $\gamma$  group was treated by 100U/mL IFN- $\gamma$  for 24 hours, combination group was treated by 100 nM TAK-981 and 100U/mL IFN- $\gamma$  for 24 hours. (C). The fluorescent median intensity for each group from (B) was calculated from FlowJo and plotted in a dot plot for statistical analysis. (D). Fluorescent median intensity peak chart of MHC-I levels in flow cytometry. The unstained control group is composed of cells mixed from all groups without anti-mouse MHC-I antibodies. The control group was treated by vehicle; the TAK-981 group was treated by TAK-981 at 100 nM for 24 hours; the IFN- $\alpha$  group was treated by 100U/mL IFN- $\alpha$  for 24 hours, the combination group was treated by 100 nM TAK-981 and 100U/mL IFN- $\alpha$  for 24 hours. (E). The fluorescent median intensity for each group from (D) was calculated from FlowJo and plotted in a dot plot for statistical analysis.

Figure 3-6. continued

B).



C).

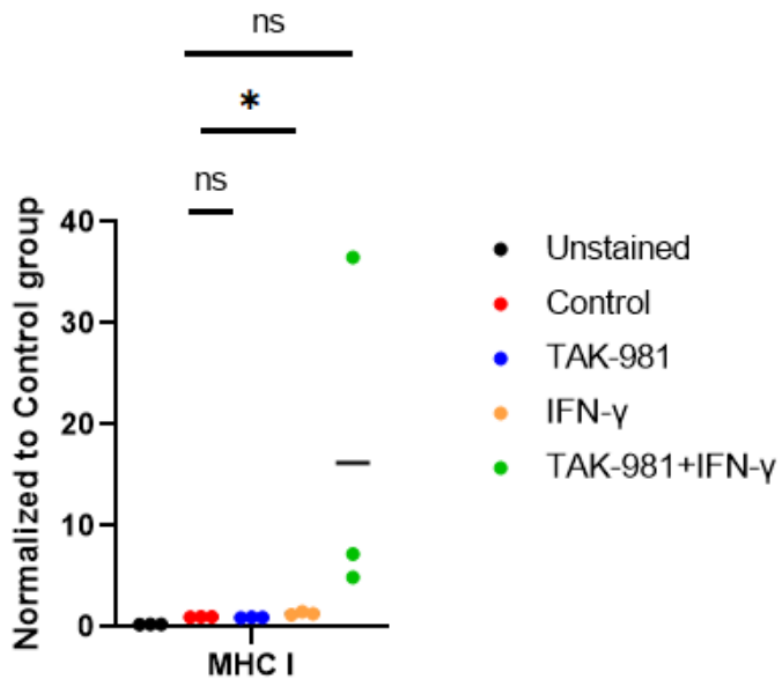
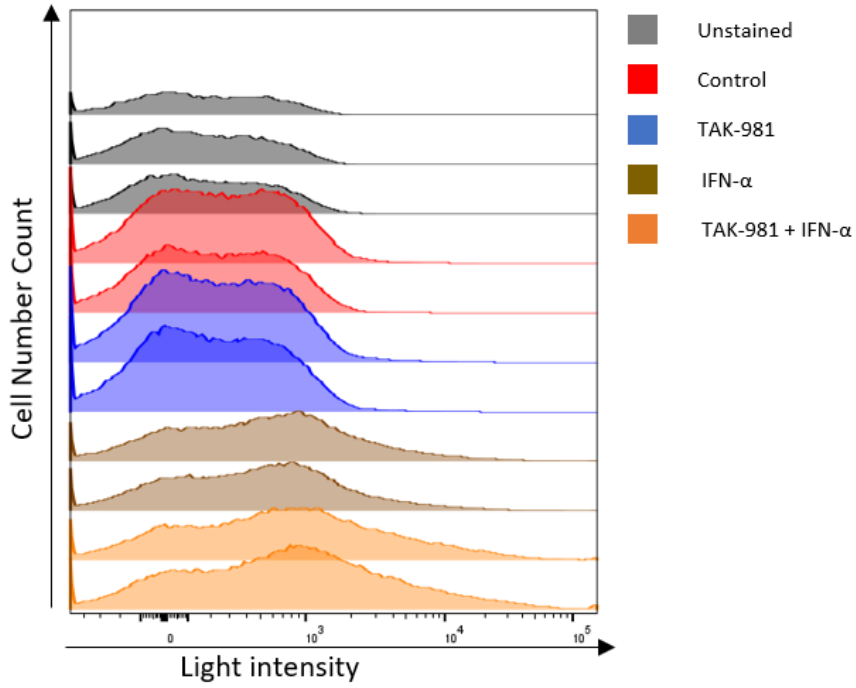
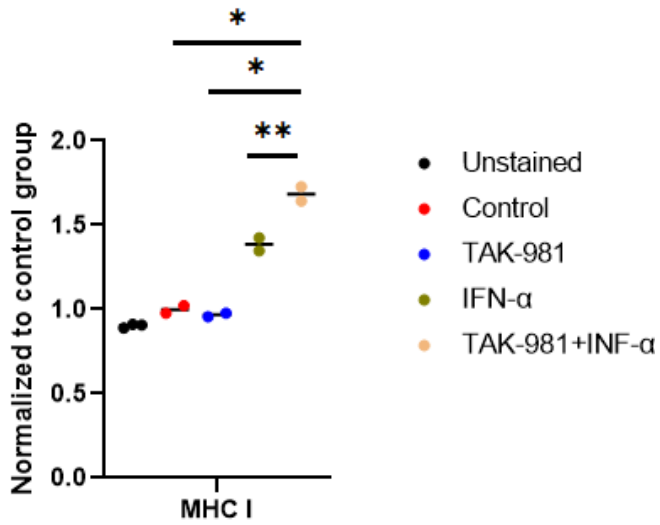


Figure 3-6. continued

D).



E).



### **3.7. Examine the combination of SUMOylation inhibition with anti-PD1 immune checkpoint inhibition**

A combination of TAK-981 and PD1 blocking immune checkpoint inhibitor (ICI) therapy is currently in a Phase II clinical trial, but head and neck cancer is not included. Therefore, I examined the effect of this combination in HNSCC models. This combination is logical scientifically because anti-PD1 ICI presumably acts on T cells, and TAK-981 monotherapy significantly improved the survival of mice with HNSCC, enhanced T cell activation, and inhibited the T cell differentiation into terminally exhausted phenotype in the tumor microenvironments.

I first treated mice with TAK-981 and anti-PD-1 ICI concurrent combination dosing in MOC1 and 4MOSC1 HNSCC-bearing mice. In MOC1 tumor-bearing mice, the concurrent combination dosing group showed better survival than the vehicle and each monotherapy group. The tumor volume versus days also showed that the combination group had significantly smaller tumor sizes compared with the anti-PD-1 group (Figure 3-7 (A) and (B)). In the TAK-981 monotherapy group, similar to what I found in the 4MOSC1 model, one of the seven mice had complete tumor regression, while the anti-PD1 monotherapy group had two out of seven complete regressions, and the combination group had three out of eight complete regressions. The combination group also had significantly increased survival. Therefore, TAK-981 and anti-PD1 ICI showed synergism in the MOC1 model.

However, in the 4MOSC1-bearing mice, I found that the therapeutic effect of combining TAK-981 and anti-PD-1 ICI therapy varies (Figure 3-7 (C), (D), and (G)). The 4MOSC1 model generally responded much better to anti-PD1 ICI than the MOC1 model. In addition, in the three independent experiments, the response to anti-PD1 depends on the number of cancer cells

implanted, although treatment started at identical tumor volumes in all experiments. The response to anti-PD1 monotherapy depends on how many tumor cells were implanted to produce the tumors, with those grown from implanting 200,000 cancer cells showing the best response (Figure 3-7 (D)) and those grown from implanting one million cancer cells showed the worst response (Figure 3-7 (F)). For mice implanted with 500,000 cancer cells, not only their response to anti-PD1 monotherapy were different over the two independent experiments, but also the combination of TAK-981 with anti-PD1 showed different outcomes with one enhanced cure rates and one reduced cure rate (Figure 3-7 (C), (D) and (G)). This finding indicates that the 4MOSC1 cell line tends to change during culturing and passage. I also investigated whether sequencing the treatments can improve efficacy. Because TAK-981 can modulate T cell differentiation, I first dosed mice with TAK-981 only, and then anti-PD-1 ICI was added, as shown in Figure 3-7 (E). Sequencing the combination of two therapies did not improve survival (Figure 3-7 (F)). Altogether, we found that TAK-981 can induce complete, durable remissions in both the 4MOSC1 and MOC1 models. However, the efficacy of combination of TAK-981 with anti-PD1 varied among different tumor models. The underlying mechanism of this variation needs to be further investigated.

A).

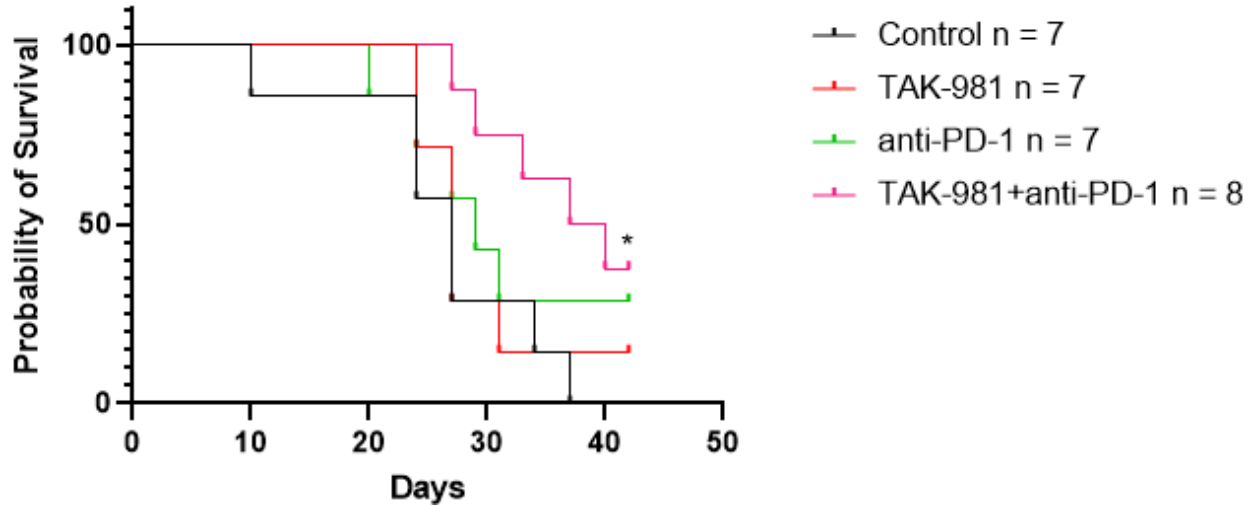
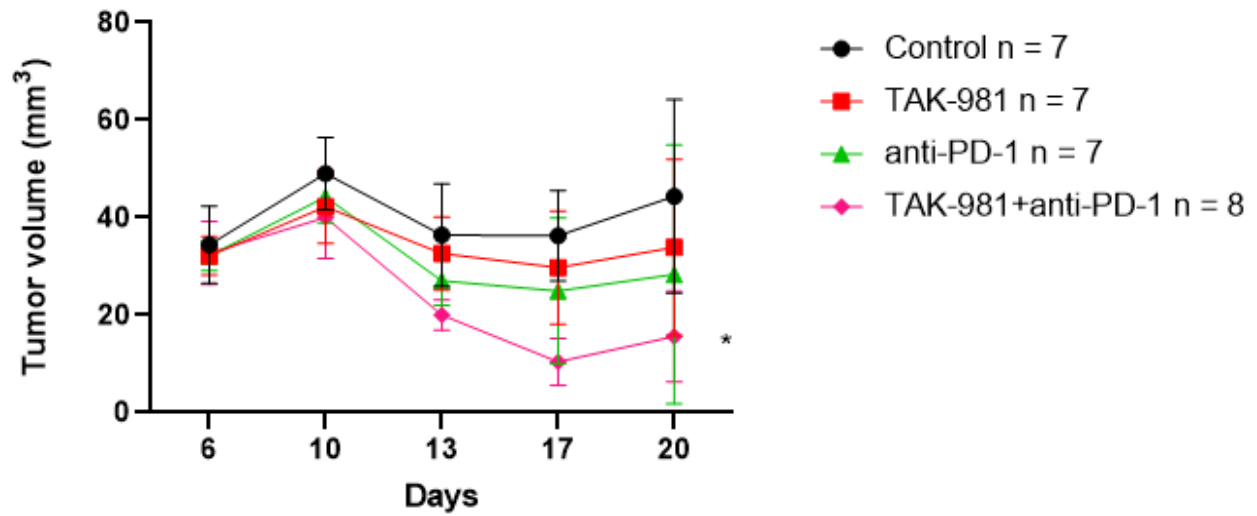


Figure 3-7. Evaluation of the efficacy of the combination of SUMOylation inhibition with anti-PD1 ICI. (A). Survival of mice that developed tumors from injecting 1 million MOC1 cells. Vehicle: vehicle-treated, TAK-981: TAK-981 treated, anti-PD1: anti-PD-1 antibodies treated, TAK-981+anti-PD1: TAK-981 and anti-PD1 treated. \*,  $p < 0.05$  when comparing the combination group with the vehicle or with the TAK-981 treated group. (B) Tumor volume vs. days of the MOC1 model in Vehicle: vehicle treated, TAK-981: TAK-981 treated, anti-PD1: anti-PD1 antibodies treated, TAK-981+anti-PD1: TAK-981 and anti-PD1 treated. \*,  $p < 0.05$  when comparing the combination group with the anti-PD1 group. (C). Survival of mice that developed tumors from injecting 500,000 4MOSC1 cells. Vehicle: vehicle treated TAK-981: TAK-981 treated, TAK-981+anti-PD-1: TAK-981 and anti-PD-1 concurrently treated. (D). Survival of mice bearing tumors developed from injection of 200,000 4MOSC1 cells. Vehicle: vehicle treated, TAK-981: TAK-981 treated, anti-PD-1: anti-PD-1 antibodies treated, TAK-981+anti-PD-1: TAK-981 and anti-PD-1 concurrently treated. (E). Treatment scheme of TAK-981 anti-PD-1 antibodies sequential strategy (F). (F). Survival of mice bearing tumors developed from injection of 1 million 4MOSC1 cells. Vehicle: vehicle treated, TAK-981: TAK-981 treated, anti-PD-1: anti-PD-1 antibodies treated, TAK-981+, then anti-PD1: TAK-981 and anti-PD-1 sequential treatment as shown in (E). (G). Survival of mice bearing tumors developed from injecting 500,000 4MOSC1 cells in anti-PD-1: anti-PD-1 antibodies treated, TAK-981+ anti-PD1: TAK-981 and anti-PD-1 treated.

Figure 3-7. continued

B).



C).

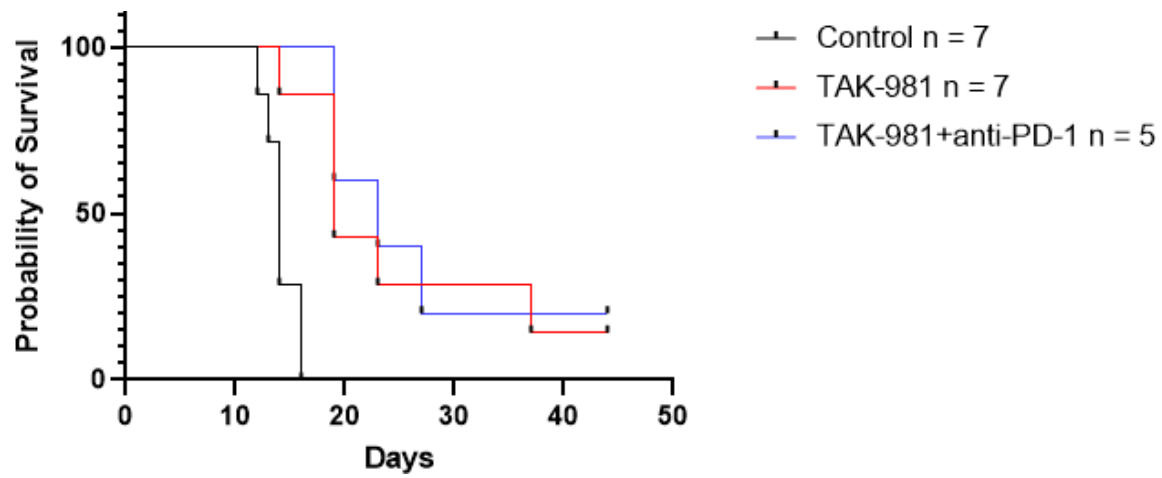
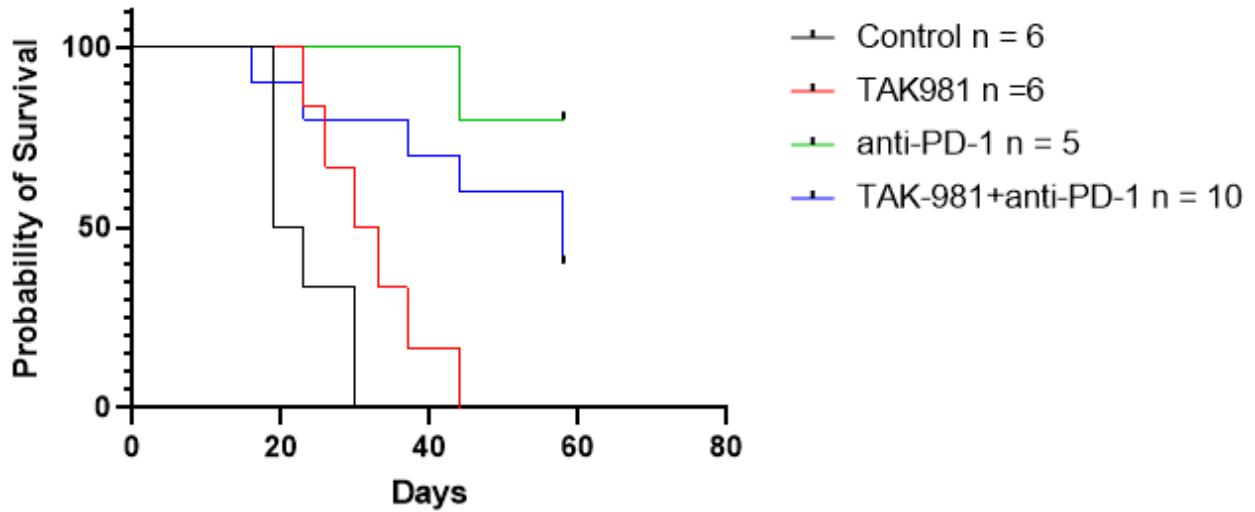


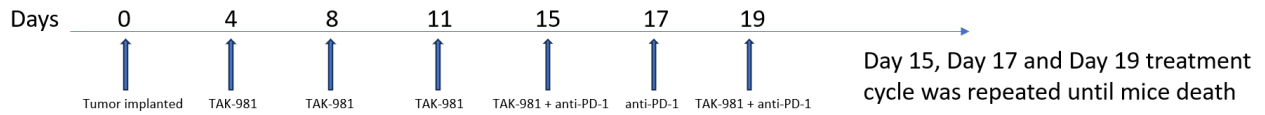
Figure 3-7. continued

D).

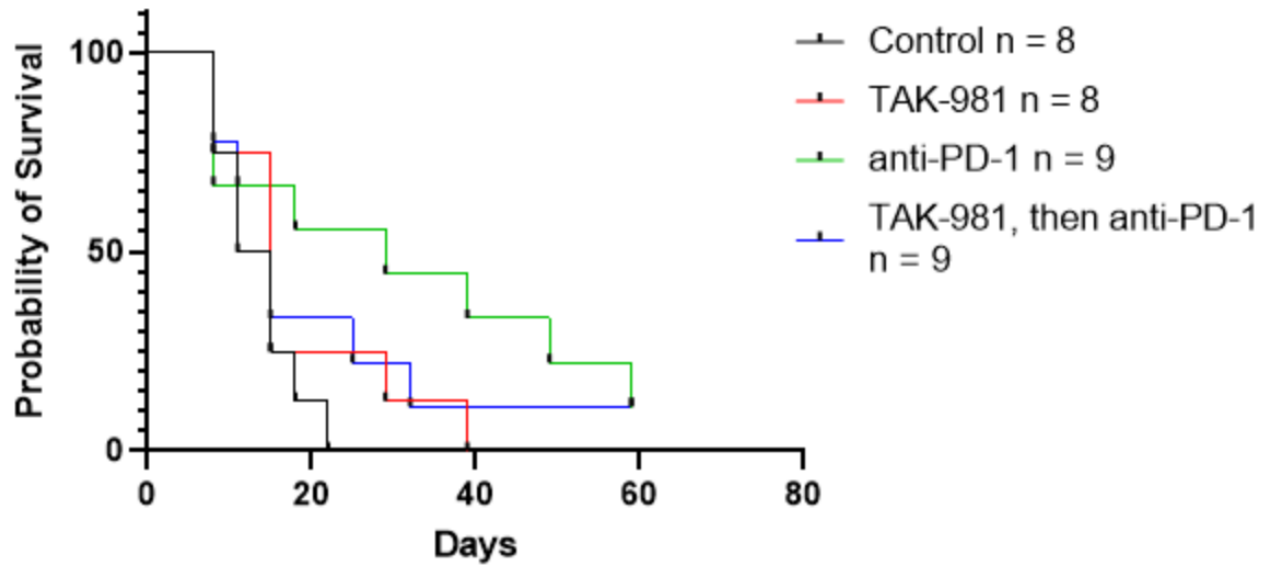


E).

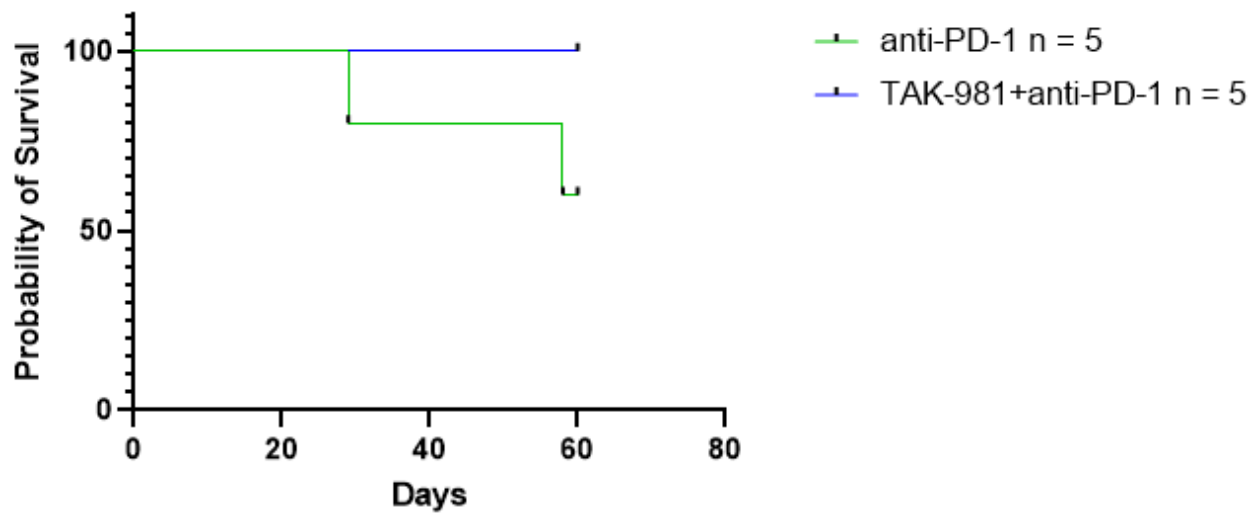
Treatment strategy for TAK-981, then anti-PD-1 sequential dosing group



F).



G).



## Chapter 4 CONCLUSIONS and FUTURE DIRECTIONS

In this study, we investigated the effect of SUMOylation inhibition on tobacco-induced head and neck cancer mouse models. SUMOylation inhibition can induce prolonged survival and can induce cures. My data demonstrated the development of adaptive immunity against tumors. The effect is likely through both tumor-cell specific and immune cell-specific mechanisms. Regarding tumor cells, I found that the MHC-I is upregulated by SUMOylation inhibition with TAK-981 *in vivo*. Because MHC-I is necessary for the presentation of neoantigen for T cell recognition and killing of tumor cells, the increase in MHC-I likely contributes to the therapeutic effects of SUMOylation inhibition. *In vitro* studies using tumor cell lines showed that SUMOylation inhibition alone did not increase MHC-I expression, but SUMOylation inhibition enhanced interferon-induced MHC-I increase. This finding suggests that the *in vivo* increase of MHC-I is likely through cytokines produced by the immune cells in the tumor microenvironment. For T cells, I found that SUMOylation inhibition reduced terminally exhausted CD8<sup>+</sup> T cells, increased effector memory T cells, and increased cytotoxic functions of effector T cells. I also investigated the combination of the SUMOylation inhibitor with an anti-PD1 antibody. Unexpectedly, I found that the effect varied among the different models.

Several questions need further investigation. The importance of MHC-I upregulation in SUMOylation-dependent therapeutic benefit needs to be demonstrated by knocking down MHC-I in tumor cells and then determining the effects on SUMOylation inhibition-mediated therapeutic benefit *in vivo*. In addition, the mechanism of how SUMOylation inhibition synergized with IFNs to increase MHC-I expression is unknown. Furthermore, how MHC-I expression changes with the duration of the exposure remains to be explored.

The lack of synergism combining TAK-981 with anti-PD-1 ICI with the 4MOSC1 model in most experiments indicates that combining one efficacious immune therapy with another efficacious immune therapy does not necessarily produce additive or synergistic effects. This finding highlights the importance of understanding the mechanism by which biomarkers are developed to predict synergism. Such studies are of timely importance because this combination is currently in clinical trials in multiple solid tumors under the assumption that I made when testing the combination in the head and neck cancer models. The synergism therapeutic effect could be tumor model dependent, but further optimizations to improve the 4MOSC1 model's reproducibility are required.

In this study, I only investigated the tumor microenvironment. Tumor-draining lymph nodes and spleen, which are also important for immune therapy response<sup>55</sup>, need further investigations. Also, more validations toward the single-cell RNA-Seq finding are needed, for example, using immunofluorescent real-time quantitative PCR on tumor tissues.

## REFERENCES

1. Celen, A.B., and Sahin, U. (2020). Sumoylation on its 25th anniversary: mechanisms, pathology, and emerging concepts. *FEBS J.* 287, 3110–3140. 10.1111/febs.15319.
2. Song, J., Durrin, L.K., Wilkinson, T.A., Krontiris, T.G., and Chen, Y. (2004). Identification of a SUMO-binding motif that recognizes SUMO-modified proteins. *Proceedings of the National Academy of Sciences* 101, 14373–14378. 10.1073/pnas.0403498101.
3. Geiss-Friedlander, R., and Melchior, F. (2007). Concepts in sumoylation: a decade on. *Nat. Rev. Mol. Cell Biol.* 8, 947–956. 10.1038/nrm2293.
4. Desterro, J.M., Rodriguez, M.S., Kemp, G.D., and Hay, R.T. (1999). Identification of the enzyme required for activation of the small ubiquitin-like protein SUMO-1. *J. Biol. Chem.* 274, 10618–10624. 10.1074/jbc.274.15.10618.
5. Johnson, E.S., and Blobel, G. (1997). Ubc9p is the conjugating enzyme for the ubiquitin-like protein Smt3p. *J. Biol. Chem.* 272, 26799–26802. 10.1074/jbc.272.43.26799.
6. Lee, G.W., Melchior, F., Matunis, M.J., Mahajan, R., Tian, Q., and Anderson, P. (1998). Modification of Ran GTPase-activating protein by the small ubiquitin-related modifier SUMO-1 requires Ubc9, an E2-type ubiquitin-conjugating enzyme homologue. *J. Biol. Chem.* 273, 6503–6507. 10.1074/jbc.273.11.6503.
7. Gong, L., and Yeh, E.T.H. (2006). Characterization of a Family of Nucleolar SUMO-specific Proteases with Preference for SUMO-2 or SUMO-3 \*. *J. Biol. Chem.* 281, 15869–15877. 10.1074/jbc.M511658200.
8. Di Bacco, A., Ouyang, J., Lee, H.-Y., Catic, A., Ploegh, H., and Gill, G. (2006). The SUMO-specific protease SENP5 is required for cell division. *Mol. Cell. Biol.* 26, 4489–4498. 10.1128/MCB.02301-05.
9. Chen, Y. (2023). A new immuno-oncology target - SUMOylation. *Trends Cancer Res.* 9, 606–608. 10.1016/j.trecan.2023.04.010.
10. Langston, S.P., Grossman, S., England, D., Afroze, R., Bence, N., Bowman, D., Bump, N., Chau, R., Chuang, B.-C., Claiborne, C., Cohen, L., Connolly, K., Duffey, M., Durvasula, N., Freeze, S., Gallery, M., Galvin, K., Gaulin, J., Gershman, R., Greenspan, P., Grieves, J., Guo, J., Gulavita, N., Hailu, S., He, X., Hoar, K., Hu, Y., Hu, Z., Ito, M., Kim, M., Lane, S.W., Lok, D., Lublinsky, A., Mallender, W., McIntyre, C., Minissale, J., Mizutani, H., Mizutani, M., Molchinova, N., Ono, K., Patil, A., Qian, M., Riceberg, J., Shindi, V., Sintchak, M.D., Song, K., Soucy, T., Wang, Y., Xu, H., Yang, X., Zawadzka, A., Zhang, J., & Pulukuri, S.M. (2021). Discovery of TAK-981, a First-in-Class Inhibitor of SUMO-Activating Enzyme for the Treatment of Cancer. *J. Med. Chem.* 64, 2501–2520. 10.1021/acs.jmedchem.0c01491.

11. Lightcap, E.S., Yu, P., Grossman, S., Song, K., Khattar, M., Xega, K., He, X., Gavin, J.M., Imaichi, H., Garnsey, J.J., Koenig, E., Zhang, H., Lu, Z., Shah, P., Fu, Y., Milhollen, M. A., Hatton, B. A., Riceberg, J., Shinde, V., Li, C., Minissale, J., Yang, X., England, D., Klinghoffer, R. A., Galvin, K., Shapiro, G., Pulukuri, S. M., Fuchs, S. Y. & Huszar, D. (2021). A small-molecule SUMOylation inhibitor activates antitumor immune responses and potentiates immune therapies in preclinical models. *Sci. Transl. Med.* *13*, eaba7791. 10.1126/scitranslmed.aba7791.
12. Chow, L.Q.M. (2020). *Head and Neck Cancer*. *N. Engl. J. Med.* *382*, 60–72. 10.1056/NEJMra1715715.
13. Siegel, R.L., Miller, K.D., Wagle, N.S., and Jemal, A. (2023). *Cancer statistics, 2023*. *CA Cancer J. Clin.* *73*, 17–48. 10.3322/caac.21763.
14. Gillison, M.L., Chaturvedi, A.K., Anderson, W.F., and Fakhry, C. (2015). Epidemiology of Human Papillomavirus-Positive Head and Neck Squamous Cell Carcinoma. *J. Clin. Oncol.* *33*, 3235–3242. 10.1200/JCO.2015.61.6995.
15. Zhang, Y., Chen, L., Hu, G., Zhang, N., Zhu, X., Yang, K., Jin, F., Shi, M., Chen, Y., Hu, W., Cheng, Z., Wang, S., Tian, Y., Wang, X., Sun, Y., Li, J., Li, W., Li, Y., Tang, L., Mao, Y. P., Zhou, G. Q., Sun, R., Liu, X., Guo, R., Long, G. X., Liang, S. Q., Li, L., Huang, J., Long, J. H., Zang, J., Liu, Q. D., Zou, L., Su, Q. F., Zhang, B. M., Xiao, Y., Guo, Y., Han, F., Mo, H. Y., Lv, J. W., Du, X. J., Xu, C., Liu, N., Li, Y. Q., Chua, M. L. K., Xie, F. Y., Sun, Y., & Ma, J. (2019). Gemcitabine and Cisplatin Induction Chemotherapy in Nasopharyngeal Carcinoma. *N. Engl. J. Med.* *381*, 1124–1135. 10.1056/NEJMoa1905287.
16. *Cancer of the oral Cavity and Pharynx - Cancer stat facts SEER*. <https://seer.cancer.gov/statfacts/html/oralcav.html>.
17. Chow, L.Q.M., Haddad, R. I., Gupta, S., Mahipal, A., Mehra, R., Tahara, M., Berger, R., Eder, J. P., Burtness, B., Lee, S., Keam, B., Kang, H., Muro, K., Weiss, J., Geva, R., Lin, C., Chung, H. C., Meister, A., Dolled-Filhart, M., Pathiraja, Kumudu., Cheng, J. D., & Seiwert, T. Y. (2016). Antitumor Activity of Pembrolizumab in Biomarker-Unselected Patients With Recurrent and/or Metastatic Head and Neck Squamous Cell Carcinoma: Results From the Phase Ib KEYNOTE-012 Expansion Cohort. *J. Clin. Oncol.* *34*, 3838–3845. 10.1200/JCO.2016.68.1478.
18. Alexandrov, L.B., Ju, Y.S., Haase, K., Van Loo, P., Martincorena, I., Nik-Zainal, S., Totoki, Y., Fujimoto, A., Nakagawa, H., Shibata, T., Campbell, P.J., Vineis, P., Phillips, D.H., & Stratton, M.R. (2016). Mutational signatures associated with tobacco smoking in human cancer. *Science* *354*, 618–622. 10.1126/science.aag0299.
19. Wang, Z., Wu, V. H., Allevato, M. M., Gilardi, M., He, Y., Martin, D., Amornphimoltham, P., McDermott, J., Yung, B. S., Goto, Y., Molinolo, A. A., Sharabi, A. B., Cohen, E. E., Chen, Q., Lyons, J. G., Alexandrov, L. B., & Gutkind, J. S. (2019). Syngeneic animal models of tobacco-associated oral cancer reveal the activity of in situ anti-CTLA-4. *Nat. Commun.* *10*, 5546. 10.1038/s41467-019-13471-0.

20. Dhatchinamoorthy, K., Colbert, J.D., and Rock, K.L. (2021). Cancer Immune Evasion Through Loss of MHC Class I Antigen Presentation. *Front. Immunol.* *12*, 636568. 10.3389/fimmu.2021.636568.
21. Palmer, K.J., Harries, M., Gore, M.E., and Collins, M.K. (2000). Interferon-alpha (IFN-alpha) stimulates anti-melanoma cytotoxic T lymphocyte (CTL) generation in mixed lymphocyte tumour cultures (MLTC). *Clin. Exp. Immunol.* *119*, 412–418. 10.1046/j.1365-2249.2000.01159.x.
22. Zhang, S., Kohli, K., Black, R.G., Yao, L., Spadinger, S.M., He, Q., Pillarisetty, V.G., Cranmer, L.D., Van Tine, B.A., Yee, C., Pierce, R.H., Riddell, S.R., Jones, R.L. & Pollack, S.M. (2019). Systemic Interferon- $\gamma$  Increases MHC Class I Expression and T-cell Infiltration in Cold Tumors: Results of a Phase 0 Clinical Trial. *Cancer Immunol Res* *7*, 1237–1243. 10.1158/2326-6066.CIR-18-0940.
23. Demel, U.M., M., Yousefian, S., Grunert, C., Zhang, L., Hotz, P. W., Gottschlich, A., Köse, H., Isaakidis, K., Vonficht, D., Grünschläger, F., Rohleder, E., Wagner, K., Dönig, J., Igl, V., Brzezicha, B., Baumgartner, F., Habringer, S., Löber, J., Chapuy, B., Weidinger, C., Kobold, S., Haas, S., Busse, A. B., Müller, S., Wirth, M., Schick, M., & Keller, U. (2022). Activated SUMOylation restricts MHC class I antigen presentation to confer immune evasion in cancer. *J. Clin. Invest.* *132*. 10.1172/JCI152383.
24. Pennock, N.D., White, J.T., Cross, E.W., Cheney, E.E., Tamburini, B.A., and Kedl, R.M. (2013). T cell responses: naive to memory and everything in between. *Adv. Physiol. Educ.* *37*, 273–283. 10.1152/advan.00066.2013.
25. Andreu-Sanz, D., and Kobold, S. (2023). Role and Potential of Different T Helper Cell Subsets in Adoptive Cell Therapy. *Cancers* *15*. 10.3390/cancers15061650.
26. Karachaliou, Gonzalez-Cao, M., Crespo, G., Drozdowskyj, A., Aldeguer, E., Gimenez-Capitan, A., Teixido, C., Molina-Vila, M. A., Viteri, S., De Los Llanos Gil, M., Algarra, S. M., Perez-Ruiz, E., Marquez-Rodas, I., Rodriguez-Abreu, D., Blanco, R., Puertolas, T., Royo, M. A., & Rosell, R. (2018). Interferon gamma, an important marker of response to immune checkpoint blockade in non-small cell lung cancer and melanoma patients. *Ther. Adv. Med. Oncol.* *10*, 1758834017749748. 10.1177/1758834017749748.
27. Brunell, A.E., Lahesmaa, R., Autio, A., and Thotakura, A.K. (2023). Exhausted T cells hijacking the cancer-immunity cycle: Assets and liabilities. *Front. Immunol.* *14*, 1151632. 10.3389/fimmu.2023.1151632.
28. Siddiqui, I., Schaeuble, K., Chennupati, V., Fuertes Marraco, S. A., Calderon-Copete, S., Pais Ferreira, D., Carmona, S. J., Scarpellino, L., Gfeller, D., Pradervand, S., Luther, S. A., Speiser, D. E., & Held, W. (2019). Intratumoral Tcf1+PD-1+CD8+ T Cells with Stem-like Properties Promote Tumor Control in Response to Vaccination and Checkpoint Blockade Immunotherapy. *Immunity* *50*, 195-211.e10. 10.1016/j.immuni.2018.12.021.
29. Miller, B.C., Sen, D. R., Al Abosy, R., Bi, K., Virkud, Y. V., LaFleur, M. W., Yates, K. B., Lako, A., Felt, K., Naik, G. S., Manos, M., Gjini, E., Kuchroo, J. R., Ishizuka, J. J., Collier,

- J. L., Griffin, G. K., Maleri, S., Comstock, D. E., Weiss, S. A., Brown, F. D., Panda, A., Zimmer, M. D., Manguso, R. T., Hodi, F. S., Rodig, S. J., Sharpe, A. H., & Haining, W. N. (2019). Subsets of exhausted CD8+ T cells differentially mediate tumor control and respond to checkpoint blockade. *Nat. Immunol.* *20*, 326–336. 10.1038/s41590-019-0312-6.
30. Jansen, C.S., Prokhnevskaya, N., Master, V. A., Sanda, M. G., Carlisle, J. W., Bilen, M. A., Cardenas, M., Wilkinson, S., Lake, R., Sowalsky, A. G., Valanparambil, R. M., Hudson, W. H., McGuire, D., Melnick, K., Khan, A. I., Kim, K., Chang, Y. M., Kim, A., Filson, C. P., Alemozaffar, M., Osunkoya, A. O., Mullane, P., Ellis, C., Akondy, R., Im, S. J., Kamphorst, A. O., Reyes, A., Liu, Y., & Kissick, H. (2019). An intra-tumoral niche maintains and differentiates stem-like CD8 T cells. *Nature* *576*, 465–470. 10.1038/s41586-019-1836-5.
  31. Hashimoto, M., Araki, K., Cardenas, M. A., Li, P., Jadhav, R. R., Kissick, H. T., Hudson, W. H., McGuire, D. J., Obeng, R. C., Wieland, A., Lee, J., McManus, D. T., Ross, J. L., Im, S. J., Lee, J., Lin, J., Hu, B., West, E. E., Scharer, C. D., Freeman, G. J., Sharpe, A. H., Ramalingam, S. S., Pellerin, A., Teichgräber, V., Greenleaf, W. J., Klein, C., Goronzy, J. J., Umaña, P., Leonard, W. J., Smith, K. A., & Ahmed, R. (2022). PD-1 combination therapy with IL-2 modifies CD8+ T cell exhaustion program. *Nature* *610*, 173–181. 10.1038/s41586-022-05257-0.
  32. Liu, Q., Sun, Z., and Chen, L. (2020). Memory T cells: strategies for optimizing tumor immunotherapy. *Protein Cell* *11*, 549–564. 10.1007/s13238-020-00707-9.
  33. Sallusto, F., Lenig, D., Förster, R., Lipp, M., and Lanzavecchia, A. (1999). Two subsets of memory T lymphocytes with distinct homing potentials and effector functions. *Nature* *401*, 708–712. 10.1038/44385.
  34. Klebanoff, C.A., Gattinoni, L., and Restifo, N.P. (2006). CD8+ T-cell memory in tumor immunology and immunotherapy. *Immunol. Rev.* *211*, 214–224. 10.1111/j.0105-2896.2006.00391.x.
  35. Berger, C., Jensen, M.C., Lansdorp, P.M., Gough, M., Elliott, C., and Riddell, S.R. (2008). Adoptive transfer of effector CD8+ T cells derived from central memory cells establishes persistent T cell memory in primates. *J. Clin. Invest.* *118*, 294–305. 10.1172/JCI32103.
  36. Fridman, W.H., Pagès, F., Sautès-Fridman, C., and Galon, J. (2012). The immune contexture in human tumours: impact on clinical outcome. *Nat. Rev. Cancer* *12*, 298–306. 10.1038/nrc3245.
  37. Plitas, G., and Rudensky, A.Y. (2016). Regulatory T Cells: Differentiation and Function. *Cancer Immunol Res* *4*, 721–725. 10.1158/2326-6066.CIR-16-0193.
  38. Kim, J.M., Rasmussen, J.P., and Rudensky, A.Y. (2007). Regulatory T cells prevent catastrophic autoimmunity throughout the lifespan of mice. *Nat. Immunol.* *8*, 191–197. 10.1038/ni1428.
  39. Ohue, Y., and Nishikawa, H. (2019). Regulatory T (Treg) cells in cancer: Can Treg cells be a new therapeutic target? *Cancer Sci.* *110*, 2080–2089. 10.1111/cas.14069.

40. Love, M.I., Huber, W., and Anders, S. (2014). Moderated estimation of fold change and dispersion for RNA-seq data with DESeq2. *Genome Biol.* *15*, 550. 10.1186/s13059-014-0550-8.
41. Hao, Y., Stuart, T., Kowalski, M.H., Choudhary, S., Hoffman, P., Hartman, A., Srivastava, A., Molla, G., Madad, S., Fernandez-Granda, C., & Satija, R. (2024). Dictionary learning for integrative, multimodal and scalable single-cell analysis. *Nat. Biotechnol.* *42*, 293–304. 10.1038/s41587-023-01767-y.
42. Seo, S.K., Choi, J.H., Kim, Y.H., Kang, W.J., Park, H.Y., Suh, J.H., Choi, B.K., Vinay, D.S., and Kwon, B.S. (2004). 4-1BB-mediated immunotherapy of rheumatoid arthritis. *Nat. Med.* *10*, 1088–1094. 10.1038/nm1107.
43. Zhu, J. (2015). T helper 2 (Th2) cell differentiation, type 2 innate lymphoid cell (ILC2) development and regulation of interleukin-4 (IL-4) and IL-13 production. *Cytokine* *75*, 14–24. 10.1016/j.cyto.2015.05.010.
44. Murphy, K., and Weaver, C. (2016). *Janeway's Immunobiology* (Garland Science).
45. Ono, M. (2020). Control of regulatory T-cell differentiation and function by T-cell receptor signalling and Foxp3 transcription factor complexes. *Immunology* *160*, 24–37. 10.1111/imm.13178.
46. Anderson, A.C., Joller, N., and Kuchroo, V.K. (2016). Lag-3, Tim-3, and TIGIT: Co-inhibitory Receptors with Specialized Functions in Immune Regulation. *Immunity* *44*, 989–1004. 10.1016/j.immuni.2016.05.001.
47. Brennan, P.J., Brigl, M., and Brenner, M.B. (2013). Invariant natural killer T cells: an innate activation scheme linked to diverse effector functions. *Nat. Rev. Immunol.* *13*, 101–117. 10.1038/nri3369.
48. Luckashenak, N., and Eisenlohr, L.C. (2013). Chapter 5 - Dendritic Cells: Antigen Processing and Presentation. In *Cancer Immunotherapy (Second Edition)*, G. C. Prendergast and E. M. Jaffee, eds. (Academic Press), pp. 55–70. 10.1016/B978-0-12-394296-8.00005-1.
49. Liao, Y., Liu, X., Huang, Y., Huang, H., Lu, Y., Zhang, Y., Shu, S., and Fang, F. (2017). Expression pattern of CD11c on lung immune cells after disseminated murine cytomegalovirus infection. *Virology* *14*, 132. 10.1186/s12985-017-0801-x.
50. Klebanoff, C.A., Gattinoni, L., Torabi-Parizi, P., Kerstann, K., Cardones, A.R., Finkelstein, S.E., Palmer, D.C., Antony, P.A., Hwang, S.T., Rosenberg, S.A., Waldmann, T.A., & Restifo, N.P. (2005). Central memory self/tumor-reactive CD8<sup>+</sup> T cells confer superior antitumor immunity compared with effector memory T cells. *Proceedings of the National Academy of Sciences* *102*, 9571–9576. 10.1073/pnas.0503726102.
51. Abu Eid, R., Ahmad, S., Lin, Y., Webb, M., Berrong, Z., Shrimali, R., Kumai, T., Ananth, S., Rodriguez, P.C., Celis, E., Janik, J., Mkrtychyan, M., & Khleif, S.N. (2017). Enhanced

Therapeutic Efficacy and Memory of Tumor-Specific CD8 T Cells by Ex Vivo PI3K- $\delta$  Inhibition. *Cancer Res.* 77, 4135–4145. 10.1158/0008-5472.CAN-16-1925.

52. Huster, K.M., Busch, V., Schiemann, M., Linkemann, K., Kerksiek, K.M., Wagner, H., and Busch, D.H. (2004). Selective expression of IL-7 receptor on memory T cells identifies early CD40L-dependent generation of distinct CD8+ memory T cell subsets. *Proc. Natl. Acad. Sci. U. S. A.* 101, 5610–5615. 10.1073/pnas.0308054101.
53. Alfei, F., Kanev, K., Hofmann, M., Wu, M., Ghoneim, H.E., Roelli, P., Utzschneider, D.T., von Hoesslin, M., Cullen, J.G., Fan, Y., Eisenberg, V., Wohlleber, D., Steiger, K., Merkler, D., Delorenzi, M., Knolle, P.A., Cohen, C.J., Thimme, R., Youngblood, B., & Zehn, D. (2019). TOX reinforces the phenotype and longevity of exhausted T cells in chronic viral infection. *Nature* 571, 265–269. 10.1038/s41586-019-1326-9.
54. Kim, S.K., and Cho, S.W. (2022). The Evasion Mechanisms of Cancer Immunity and Drug Intervention in the Tumor Microenvironment. *Front. Pharmacol.* 13, 868695. 10.3389/fphar.2022.868695.
55. Saddawi-Konefka, R., O’Farrell, A., Faraji, F., Clubb, L., Allevato, M., Jensen, S. M., Yung, B. S., Wang, Z., Wu, V. H., Anang, N. A., Msari, R. A., Schokrpur, S., Franiak-Pietryga, I., Molinolo, A. A., Mesirov, J. P., Simon, A. B., Fox, B. A., Bui, J. D., Sharabi, A. B., Cohen, E. E. W., Califano, & J., Gutkind, J. S. (2022). Lymphatic-preserving treatment sequencing with immune checkpoint inhibition unleashes cDC1-dependent antitumor immunity in HNSCC. *Nat. Commun.* 13, 4298. 10.1038/s41467-022-31941-w.